Advanced Steel Construction – Vol. 20 No. 4 (2024) 345–363
DOI:10.18057/IJASC.2024.20.4.3

INTERFACE SHEAR DEMAND AND DESIGN OF PARTIALLY CONCRETE-FILLED STEEL TUBULAR COLUMNS WITH TRANSVERSE DIAPHRAGMS

Jian Jiao [1], Yao-Jun Zhang [2] and Dan Gan [3, *]

[1] *College of Water & Architectural Engineering, Shihezi University, Shihezi 832003, China*
[2] *School of Civil Engineering, Chongqing University, Chongqing 400045, China*
[3] *School of Civil Engineering and Geomatics, Southwest Petroleum University, Chengdu 610500, China*
** (Corresponding author: E-mail: gandan@swpu.edu.cn)*

ABSTRACT

A partially concrete-filled steel tubular (CFST) column is formed by partially filling a steel hollow section (SHS) with concrete, its interface shear demand between the infilled concrete and steel tube is important in design but not usually considered. In this work, a refined finite element (FE) model of circular partially CFST columns with transverse diaphragms was established, followed by parameter analysis of the behavior under the combined axial compression and lateral loads. The main variables included the concrete filling ratio, axial compression ratio, diameter-to-thickness ratio of steel tubes, section size, aspect ratio, and material strength. The results indicate that the optimal filling ratio increases with the axial compression ratio, diameter-to-thickness ratio, and concrete strength, but decreases with the steel strength. Then, calculation methods for the optimal filling ratio, predicting the load capacity of transverse diaphragms, and the interface shear demand between the steel tube and infilled concrete were proposed. Finally, a design procedure for partially CFST columns with transverse diaphragms was proposed.

ARTICLE HISTORY

Received: 26 April 2024
Revised: 3 July 2024
Accepted: 8 July 2024

KEYWORDS

Composite structure;
Finite element analysis;
Optimal filling ratio;
Shear demand;
Transverse diaphragm

1. Introduction

A partially concrete-filled steel tubular (CFST) column is a hollow steel tubular column that is partially filled with concrete. Partially CFST columns developed as a retrofitting measure for piers initially as depicted in Fig. 1[1], which effectively reinforces the potential plastic hinge area at the bottom of the piers in an economical manner. Partially CFST columns exhibit high lateral load capacity, good ductility, and excellent energy dissipation capacity [2-11], making them widely utilized in bridge piers for both post-earthquake repair of existing bridges and construction of new bridges [12-14].

In recent decades, the seismic performance of partially CFST columns have been extensively investigated. Yuan et al. [15-16] illustrated that infilled concrete can enhance the seismic performance of steel piers when subjected to both unidirectional and bidirectional seismic forces. Goto et al. [17-18] introduced a discrete crack model, which aimed at exploring the failure mechanism of partially CFST columns, specifically the development of plastic hinges at the bottom of the column. Lai and Varma [19] performed FE analysis to study how the seismic performance of hollow spiral welded pipes is influenced by the concrete filling ratio. The findings suggested that a higher concrete filling ratio can postpone the local buckling and fracture of steel tubes. Additionally, Xiang et al. [20] indicated that the concrete filling ratio can be used as an optimization design to achieve a balance between structural performance and load capacity.

The concrete filling ratio should be designed as larger than the optimal ratio, which is defined as the minimum concrete filling ratio at which a partially CFST column can achieve the load capacity of a CFST column. Khalifa et al. [21] demonstrated that, circular partially CFST columns (f_y=280MPa, D/t=101) can achieve the load capacity equivalent to 78% of CFST columns under the concrete filling ratio of 39%, with the failure mode being local buckling at the end of the hollow part. However, Wang et al. [22] showed that when the concrete filling ratio of a circular partially CFST pier with a transverse diaphragm with similar parameters (f_y=315MPa, D/t=119) was equal to or greater than 33%, the specimen failed at the bottom of the bridge pier, exhibiting good seismic performance. The difference between the above two researches mainly lies in whether the transverse diaphragm is installed or not. Therefore, it is necessary to take certain measures to effectively transfer the load from the steel tube to infilled concrete, which can affect the optimal filling ratio and structural behavior of partially CFST columns.

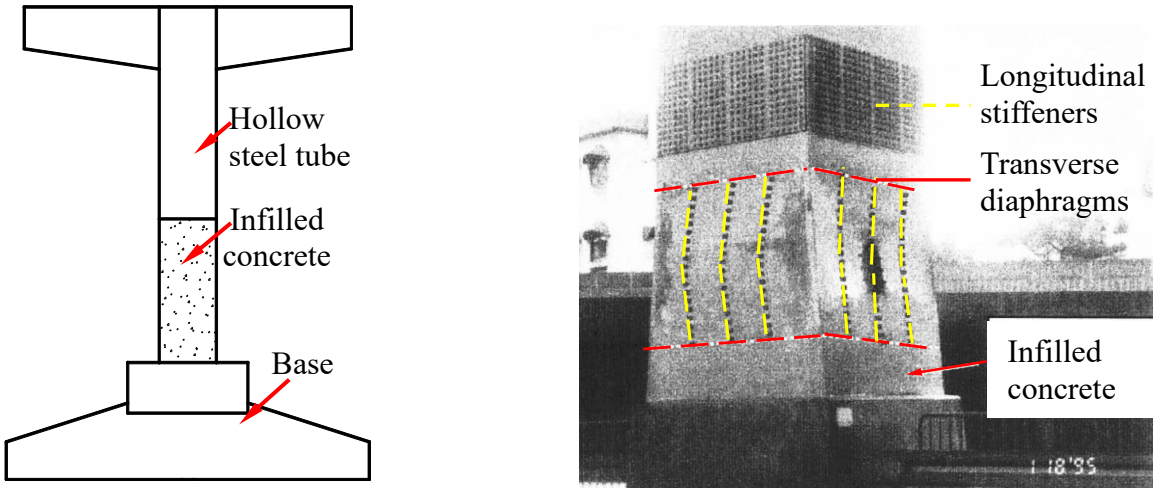

(a) Partially CFST columns pier (b) Partially CFST pier in practice [1]

Fig. 1 Partially CFST columns piers

In order to enhance the interface shear capacity and composite effect of partially CFST columns, transverse diaphragms, longitudinal stiffeners, or a combination of both were deemed essential, as illustrated in Fig. 2. Usami et al. [23-24] conducted seismic test of rectangular partially CFST piers, and the

results indicated that stiffening ribs effectively increased the strength, stiffness, deformation capacity, and energy dissipation performance of the columns. Then, Ge and Usami [25] illustrated that transverse diaphragms were similarly successful in enhancing the seismic performance of the partially CFST piers. Kwon et al. [26] concluded that longitudinal stiffening ribs could increase the load capacity of partially CFST piers beyond the sum of the capacities of the steel tube, stiffening ribs, and concrete, demonstrating a favorable composite effect. However, the design and detailing of transverse diaphragms in partially CFST columns were not discussed or analyzed, such as the mechanism of these diaphragms resists the interface shear and the interface shear demand, which is important for proposing the design methods.

The transverse diaphragm can effectively transfer the load from steel tube to infilled concrete and can be conveniently welded as shown in Fig. 3, so they facilitate utilizing the performance of the infilled concrete and have been widely used in practice. Two fundamental design parameters for the transverse diaphragm include the shear demand in partially CFST columns, as well as the load capacity of the diaphragm. Although both academic researches and practical projects adopt transverse diaphragms in partially CFST columns, the interface shear demand, design of diaphragms, and the selection of the optimal filling ratio needs to be systematically investigated for better guiding the design.

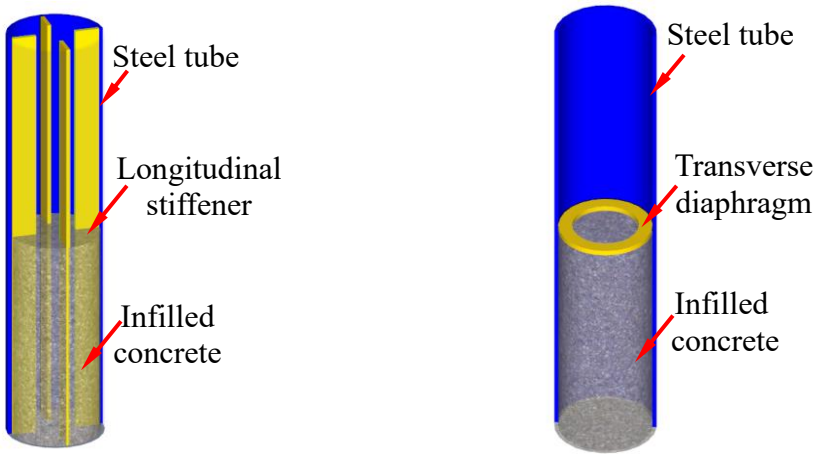

(a) With longitudinal stiffeners (b) With transverse diaphragm

Fig. 2 The stiffening measures of partially CFST columns

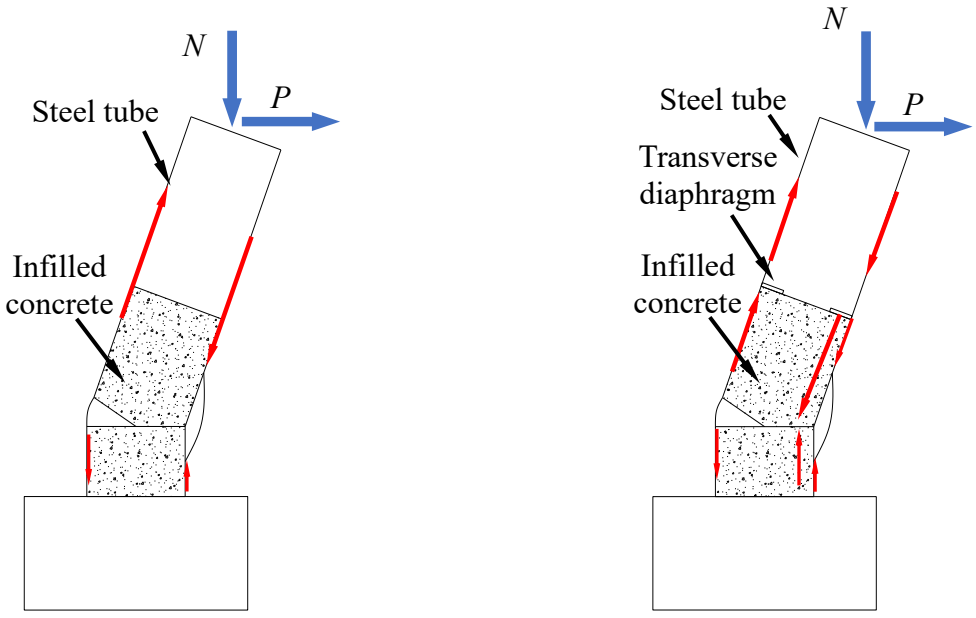

(a) Without transverse diaphragm (b) With transverse diaphragm

Fig. 3 The force transmission effect of the transverse diaphragm

In this study, a FE analysis model of partially CFST columns was established and verified, followed by parameter analysis of the behavior under the combined axial compression and lateral loads. The main parameters contained the concrete filling ratio, axial compression ratio, diameter-to-thickness ratio of steel tubes, section size, aspect ratio, and material strength. Then, a calculation method for the optimal filling ratio, predicting the load capacity of transverse diaphragms. and the shear demand between the steel tube and infilled concrete were proposed. Finally, a design procedure was proposed.

2. Nonlinear analysis

2.1. Model description

The model was established by using the software ABAQUS. The eight-node linear hexahedral element (C3D8R) was used for the steel tubes, concrete, and transverse diaphragms. Through sensitivity analysis of the mesh size, the element division size was set to one-tenth of the cross-sectional width [27]. Surface-to-surface contact interactions were established between the steel tube and infilled concrete, as well as between the transverse diaphragms and concrete. Finite sliding was used in the contacts, with its normal behavior being modeled as hard contact and its tangential behavior being represented by penalty functions incorporating a friction coefficient of 0.6 [28]. The transverse diaphragms were connected using “tie” constraints. The FE model and boundary conditions are shown in Fig. 4. The top surface of the column was coupled to point RP-1, where the load was applied; the bottom surface of the partially CFST column was fixed and coupled to point RP-2.

A steel model followed an elastic-perfectly plastic model, as shown in Eq. (1), featuring an elastic modulus (E_s) of 2.06×105 MPa and a Poisson’s ratio of 0.3. The concrete was characterized by an elastic modulus (E_c) of 4700fc0.5 [29] and a Poisson’s ratio of 0.2, as shown in Eq. (2). A plastic damage model [30] was implemented for the concrete, incorporating the specific parameters detailed in Table 1. To characterize the tensile behavior of concrete, a fracture energy

model was employed, defining the tensile stress f_t by the Ref. [31] and tensile fracture energy Gf as suggested in the CEB-FIP MC90 [32], as defined in Eq. (3) and Eq. (4).

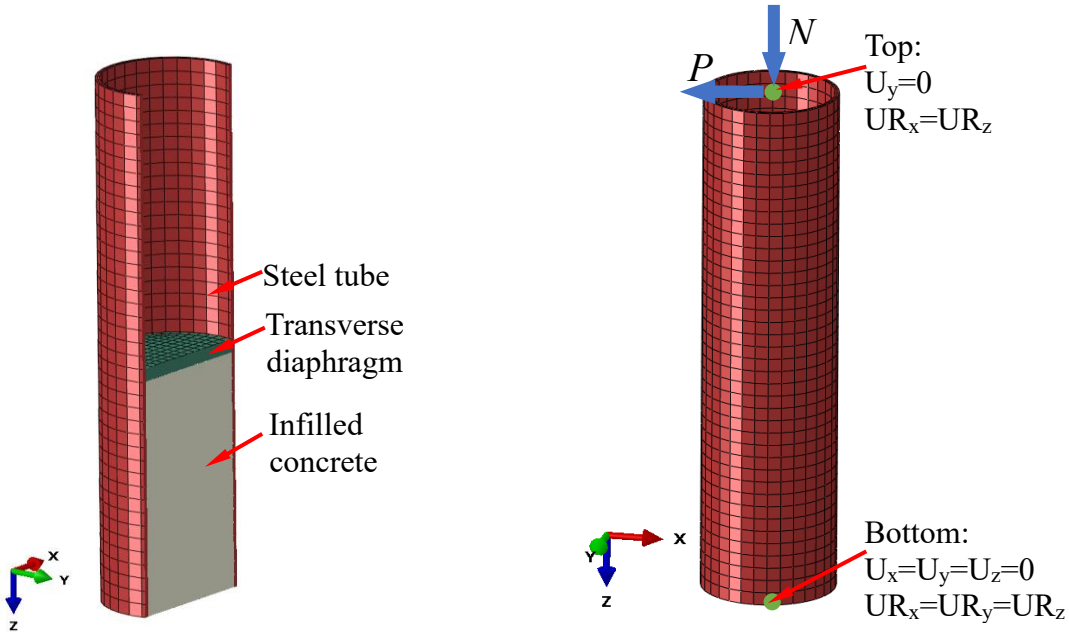

Fig. 4 FE model and boundary conditions

$$\sigma = \begin{cases} E_s\varepsilon, & (\varepsilon \le \varepsilon_y) \\ f_y, & (\varepsilon > \varepsilon_y) \end{cases} \quad (1)$$

where E_s is the elastic modulus of steel; f_y and ε are the yield stress and strain of steel, respectively.

$$y = \begin{cases} 2x - x^2, & (x \le 1) \\ \dfrac{x}{\beta_0(x-1)^\eta + x}, & (x > 1) \end{cases} \quad (2)$$

where $x = \varepsilon/\varepsilon_0$; $y = \sigma/\sigma_0$; $\sigma_0 = f_c'$; $\beta_0 = (f_c')/1.2\sqrt{1+\xi}$; $\xi = A_s f_y/A_c f_{ck}$; $\eta = 1.6 + 1.5/x$; $f_{ck} = 0.642 f_{cu}$; $f_c' = 0.833 f_{cu}$; $\varepsilon_0 = \varepsilon_c + 800\xi^{0.2} \times 10^{-6}$; $\varepsilon_c = (1300 + 12.5 f_c') \times 10^{-6}$.

Table 1
Concrete parameter values

ψ	e	f_{b0}/f_{c0}	K_c	μ
38°	0.1	1.16	0.667	0.0001

$$f_t = 0.375 f_{cu}^{0.55} \quad (3)$$

$$G_f = \alpha(0.1 f_c)^{0.7} \quad (4)$$

where α is related to the size of concrete aggregates, taken as 0.03.

2.2. Model verification

To verify the accuracy of the FE analysis models, the experimental results of partially CFST columns under bending load [21] were selected and compared. The comparison of the failure modes is depicted in Fig. 5. The circular partially CFST column displayed plastic hinge formation at the end of the hollow section, with the simulated failure mode aligning closely with the experimental results. Meanwhile, the load-displacement curves depicted in Fig. 6 illustrated a good agreement between the FE analysis results and the experimental results.

(a) The failure mode of T160-16

(b) The FE result

Fig. 5 Comparison of failure mode

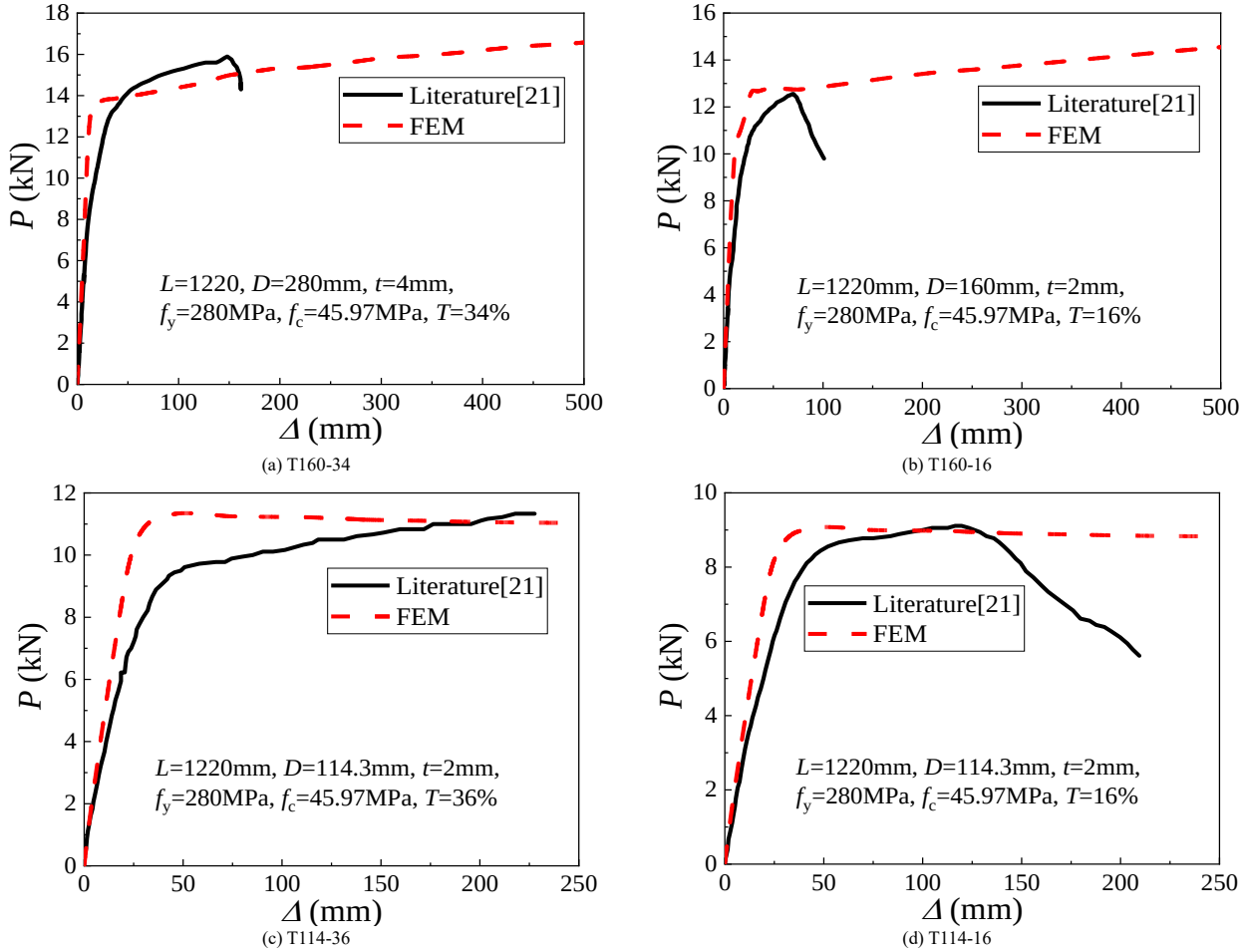

Fig. 6 Comparison of load-displacement curves between FE analysis and experiments

2.3. Parameter analysis

2.3.1. Parameter matrix

The models were subjected to combined axial compression and lateral loading. 440 FE models were designed, and the analysis parameters are listed in Table 2. Model designation conventions are explained using "n2-q235-4-33-40-30%" as an example: "n2" signifies an axial compression ratio of n=0.2 (where $n=N/(f_yA_s)$, A_s is the cross-sectional area of the steel tube), "q235" indicates a steel yield strength of 235 MPa, "4" represents an aspect ratio of L/D = 4, "33" represents a steel tube diameter-to-thickness ratio of D/t = 33, "40" denotes a cubic compressive strength of f_{cu}=40 MPa, and "30%" indicates a concrete filling ratio (T) of 30%.

The concrete filling ratio (T) ranged from 0% to 95%, with models established at 5% intervals. Using a binary search method, the optimal filling ratio, i.e., the minimum concrete filling ratio at which a partially CFST column basically reaches the load capacity of a CFST column, is determined with a precision of one hundredth of a percent.

In order to ensure that the transverse diaphragm is sufficient to transfer the load to the concrete, the diaphragm was set as a solid plate, and the thickness of the transverse diaphragm was calculated based on the axial compressive load capacity of the steel tube as the shear resistance. The material properties were the same as the steel tube.

Table 2
Main design parameters of the partially CFST models

Model Number	Main design parameters					
	Steel tube outer diameter D (mm)	Steel tube thickness t (mm)	Aspect ratio L/D	Concrete strength f_{cu}（MPa）	Steel strength f_y（MPa）	Axial compression ratio n
n1-q235-200-4-33-40-(0–95)	200	6	4	40	235	0.1
n2-q235-200-4-33-40-(0–95)	200	6	4	40	235	0.2
n3-q235-200-4-33-40-(0–95)	200	6	4	40	235	0.3
n4-q235-200-4-33-40-(0–95)	200	6	4	40	235	0.4
n5-q235-200-4-33-40-(0–95)	200	6	4	40	235	0.5
n6-q235-200-4-33-40-(0–95)	200	6	4	40	235	0.6
n2-q235-400-4-33-40-(0–95)	400	12	4	40	235	0.2
n2-q235-600-4-33-40-(0–95)	600	18	4	40	235	0.2
n2-q235-800-4-33-40-(0–95)	800	24	4	40	235	0.2
n2-q235-200-4-20-40-(0–95)	200	10	4	40	235	0.2
n2-q235-200-4-25-40-(0–95)	200	8	4	40	235	0.2
n2-q235-200-4-50-40-(0–95)	200	4	4	40	235	0.2
n2-q235-200-8-33-40-(0–95)	200	6	8	40	235	0.2

n2-q235-200-12-33-40-(0–95)	200	6	12	40	235	0.2
n2-q235-200-16-33-40-(0–95)	200	6	16	40	235	0.2
n2-q355-200-4-33-40-(0–95)	200	6	4	40	355	0.2
n2-q460-200-4-33-40-(0–95)	200	6	4	40	460	0.2
n2-q690-200-4-33-40-(0–95)	200	6	4	40	690	0.2
n2-q235-200-4-33-20-(0–95)	200	6	4	20	235	0.2
n2-q235-200-4-33-30-(0–95)	200	6	4	30	235	0.2
n2-q235-200-4-33-50-(0–95)	200	6	4	50	235	0.2
n2-q235-200-4-33-60-(0–95)	200	6	4	60	235	0.2

2.3.2. Failure modes

The influence of the concrete filling ratio on the failure modes follows a similar pattern in different models, represented by models n2-q235-4-33-40-(0–95%).

As shown Fig. 7(a), at a concrete filling ratio of 0 (i.e., steel hollow tube), the failure mode is characterized by plastic buckling at the bottom of the steel tube. With increasing concrete filling ratio (0% to 10%), the failure mode changes to plastic buckling of the steel hollow section (SHS) above the steel-concrete interface, resulting in increased load capacity and ductility, as shown in Fig. 7(b). When the concrete filling ratio increased to the range of 10% to 28%, as depicted in Fig. 7(c), the failure mode changes from buckling of the SHS to plastic hinge formation at the bottom of the column. This indicates that the optimal filling ratio is 28%. Beyond the optimal filling ratio, the failure mode is the same as shown in Fig. 7(d). As the concrete filling ratio further increases, the stiffness slightly improves, while the load capacity and ductility barely change, as shown in Fig. 8.

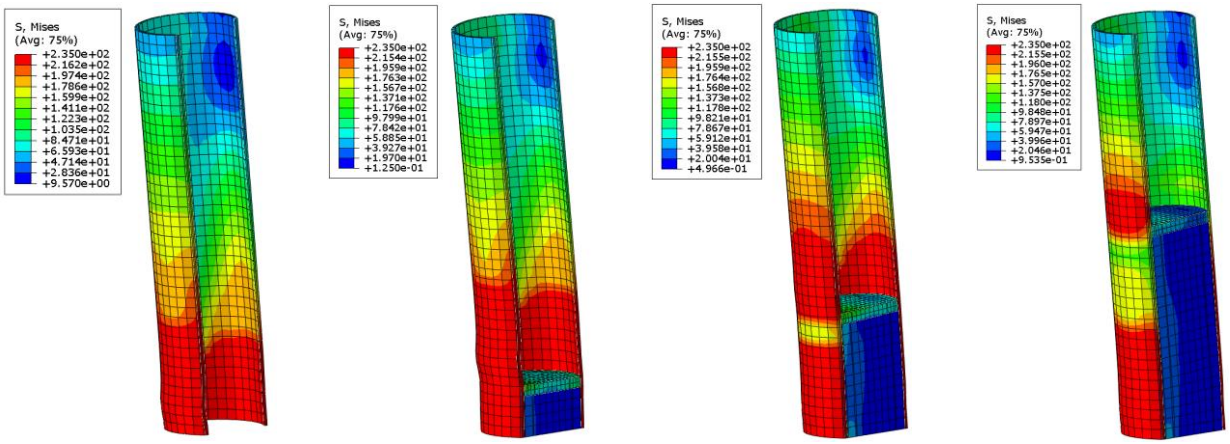

(a) T =0% (b) T=10% (c) T=28% (d) T=50%

Fig. 7 Failure modes of partially CFST columns under different concrete filling ratios

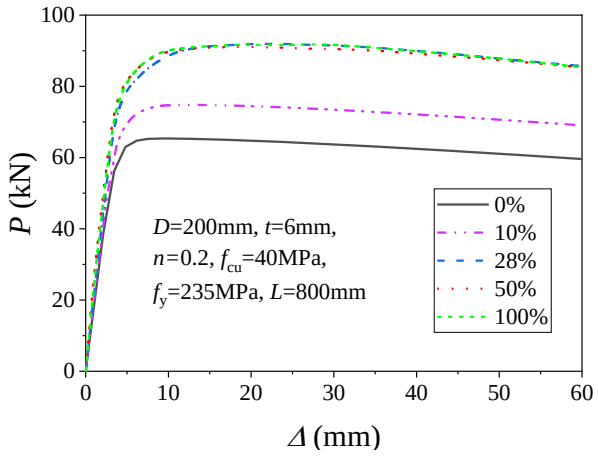

Fig. 8 Load-displacement curves of partially CFST columns with different concrete filling ratios

2.3.3. Parametric analysis

Before analyzing the impact of various parameters on the optimal filling ratio, it is necessary to clarify that, as explained in Section 2.3.2, when the optimal filling ratio is achieved, the failure mode of the partially CFST column is characterized by the formation of plastic hinges at both the base of the column and the SHS above the steel-concrete interface. Both sections reach their combined compressive and bending load capacity.

At this point, if the strength of the composite section enhances, the lateral load will also increase, while the strength of SHS remains unchanged, which will cause the failure of the hollow steel tube. To ensure the failure mode mentioned earlier, the concrete filling height will increase, so the optimal filling ratio will increase, as shown in Fig. 9(a). Conversely, if the strength of the SHS increases, the SHS will not fail. To achieve the desired failure mode, the height of concrete filling should be reduced, resulting in a decrease in the optimal filling ratio, as shown in Fig. 9(b), in which M_s and M_{sc} represent the compression-bending capacity of the SHS and the composite section, respectively. In addition, M_{s1} and M_{sc1} represent the compression-bending capacity of the strengthened SHS and composite section, respectively. From this analysis, it can be concluded that the optimal filling ratio is related to the relative strength of the SHS and the composite section. When the load capacity of the composite section increases more significantly compared to the SHS, the optimal filling ratio decreases, and vice versa.

(1) Axial compression ratio

When the axial compression ratio ranges from 0.1 to 0.6, the lateral load capacity decreases with an increase in the axial compression ratio (Fig. 10(a)). Once the optimal filling ratio is reached, the load capacity basically un-changes,

at the optimal filling ratio, the differences in the load capacity among the columns decrease. This is because before reaching the optimal filling ratio, the failure occurs in the SHS above the concrete interface, and the influence of axial compression ratio on the steel tube is obvious; when the optimal filling ratio is reached, the composite section of the column base fails, while the influence of axial force is relatively small.

The optimal filling ratio increases with the axial compression ratio as depicted in Fig. 10(b). This is also because when the axial force increases, the compressive and bending load capacity of the composite section decreases less than the SHS. The relationship between the axial compression ratio and the compression-bending capacity of the sections can be determined based on the *N-M* curve, as shown in Fig. 11(a), and the load capacity ratios of the two sections under different axial compression ratios are shown in Fig. 11(b). It can be observed that as the axial compression ratio increases, the compression-bending capacity of the composite section becomes relatively stronger compared to the unfilled steel tube section, resulting in an increase in the optimal filling ratio.

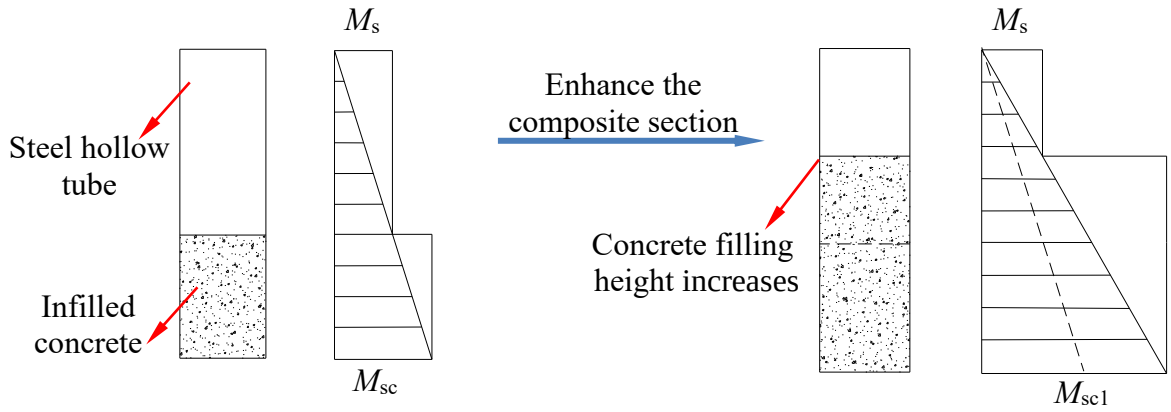

(a) Optimal filling ratio increases with a stronger composite section

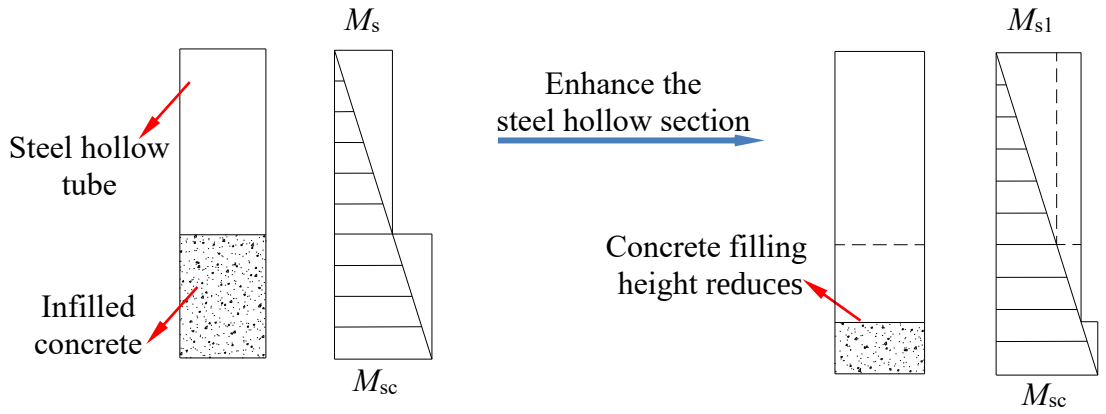

(b) Optimal filling ratio decreases with a stronger steel hollow section

Fig. 9 The influence of two types of sections strength on the optimal filling ratio

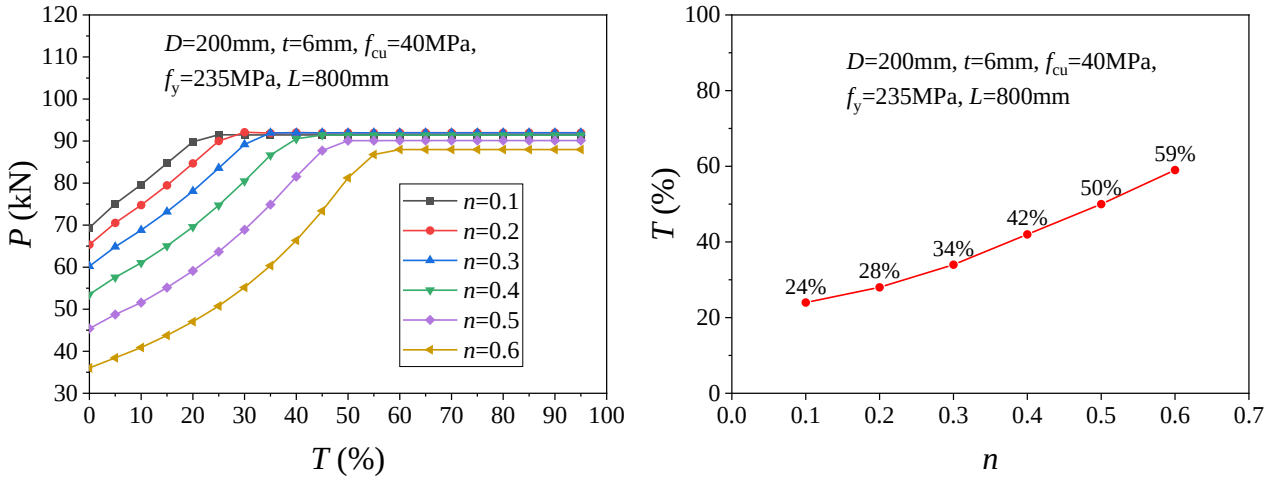

(a) Load capacity-filling ratio curves

(b) Optimal filling ratio under different axial compression ratios

Fig. 10 Effect of axial compression ratio on the load capacity and optimal filling ratio

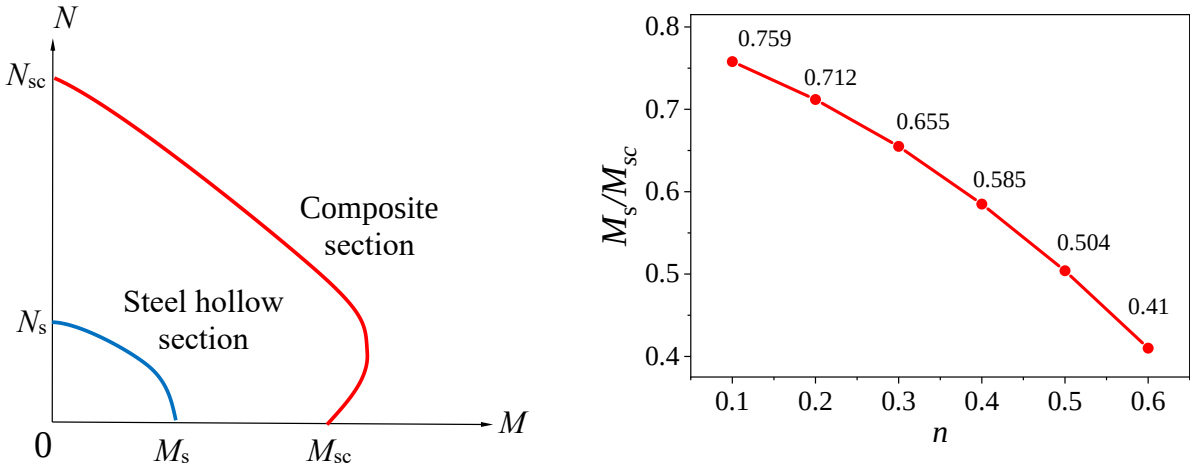

(a) Comparison of *N-M* curves for two sections (b) The ratio of load capacity decreases with axial compression ratios

Fig. 11 Effect of vertical load on the load capacity of SHS and composite section

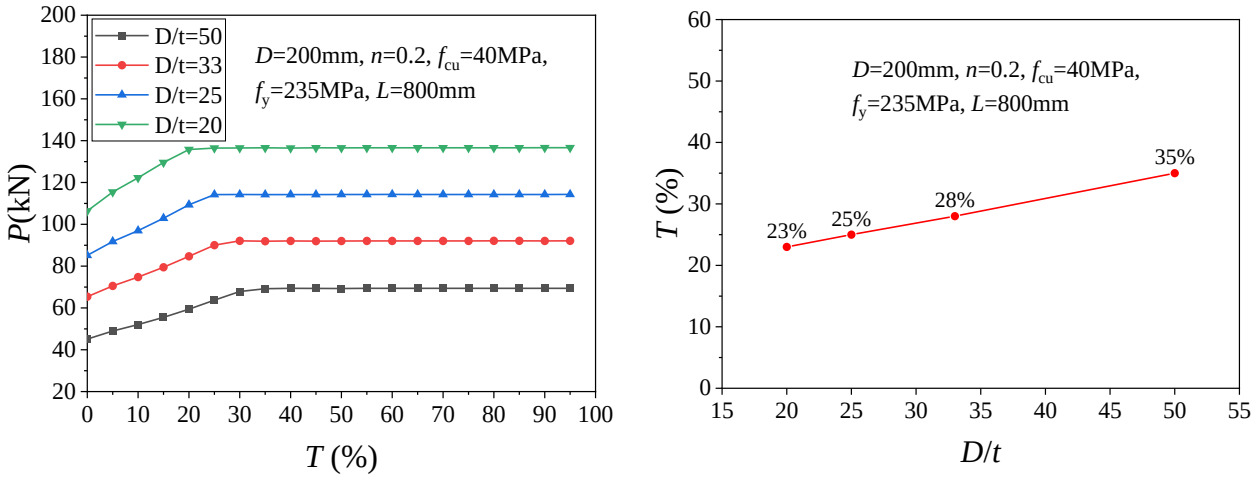

(a) Load capacity-concrete filling ratio curves (b) Optimal filling ratio under different diameter-to-thickness ratios

Fig. 12 Effect of diameter-to-thickness ratio on the load capacity and optimal filling ratio

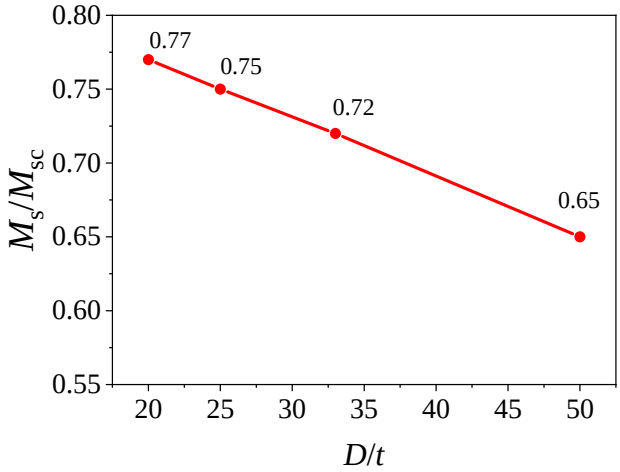

Fig. 13 The ratio of load capacity decreases with diameter-to-thickness ratios

(2) Diameter-to-thickness ratio

When the diameter-to-thickness ratio ranges from 20 to 50, the lateral load capacity decreases with an increase in the diameter-to-thickness ratio (Fig. 12(a)). This is because as the ratio of diameter-to-thickness increases, the strength of the composite section decreases, resulting in a corresponding decrease in load capacity of columns at every concrete filling ratio.

The optimal filling ratio increases with the diameter-to-thickness ratio (Fig. 12(b)). This is because when the steel tube thickness reduces, the compression-bending capacity of the SHS reduced more, as shown in Fig. 13.

(3) Steel strength

Fig. 14 (a) depicts that the lateral load capacity of steel tubes increases with the increase of steel strength in the range of 235MPa to 690MPa. This is because the increase of steel tube strength enhances the compressive-bending load capacity of the composite section.

Fig. 14(b) illustrates the optimal filling ratio increases with increasing steel strength. This is attributed to the fact that as the steel strength increases, the compression-bending capacity of the composite section increases relatively smaller than that of the SHS, as shown in Fig. 15.

(4) Concrete strength

When the concrete strength ranges from 20MPa to 60MPa, there is no difference in lateral load capacity before reaching the optimal filling ratio (Fig. 16(a)). However, once the optimal filling ratio is achieved, the load capacity increases with higher concrete strength. This is because the concrete strength is only related to the load capacity of the composite section. Therefore, when the SHS is damaged, the load capacity of every CFST column is consistent. When the composite section is damaged, the load capacity of the section increases with the increase of concrete strength.

The optimal filling ratio increases with increasing concrete strength (Fig.

16(b)). This is attributed to the fact that as the concrete strength increases, the load capacity of the composite section is enhanced.

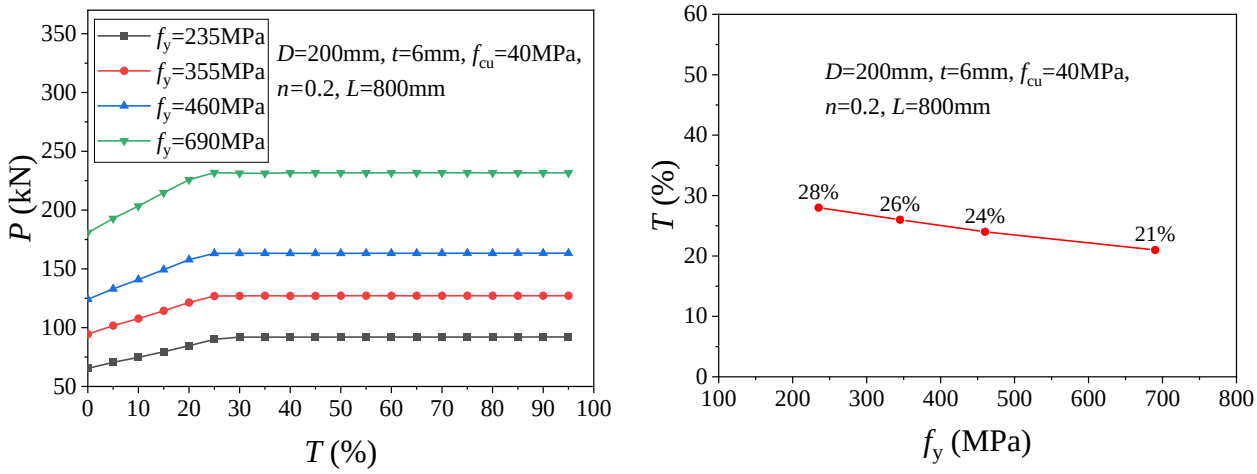

(a) Load capacity-concrete filling ratio curves (b) Optimal filling ratio under different steel strengths

Fig. 14 Effect of steel strength on the load capacity and optimal filling ratio

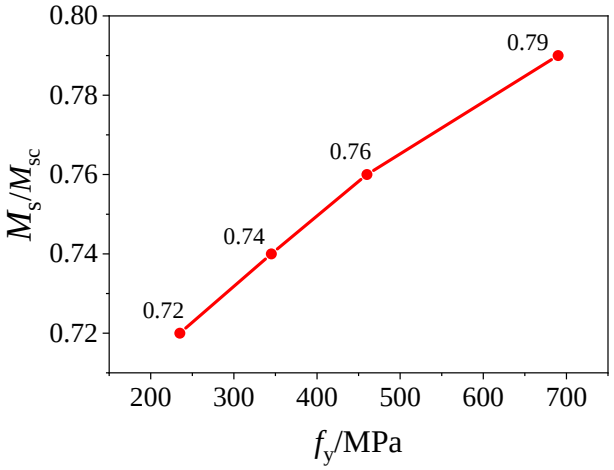

Fig. 15 The ratio of load capacity increases with steel strengths

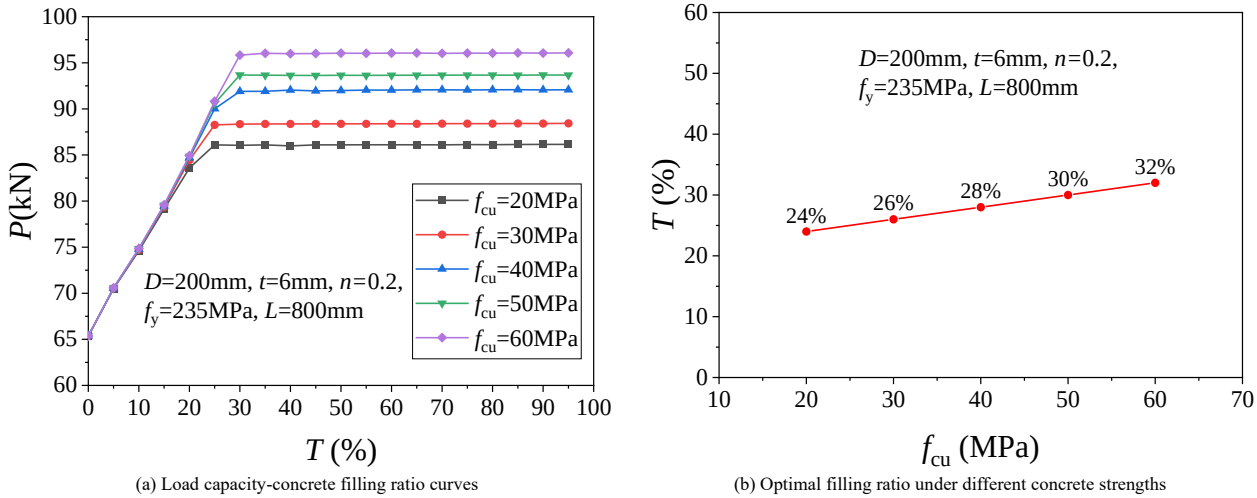

(a) Load capacity-concrete filling ratio curves (b) Optimal filling ratio under different concrete strengths

Fig. 16 Effect of concrete strength on the load capacity and optimal filling ratio

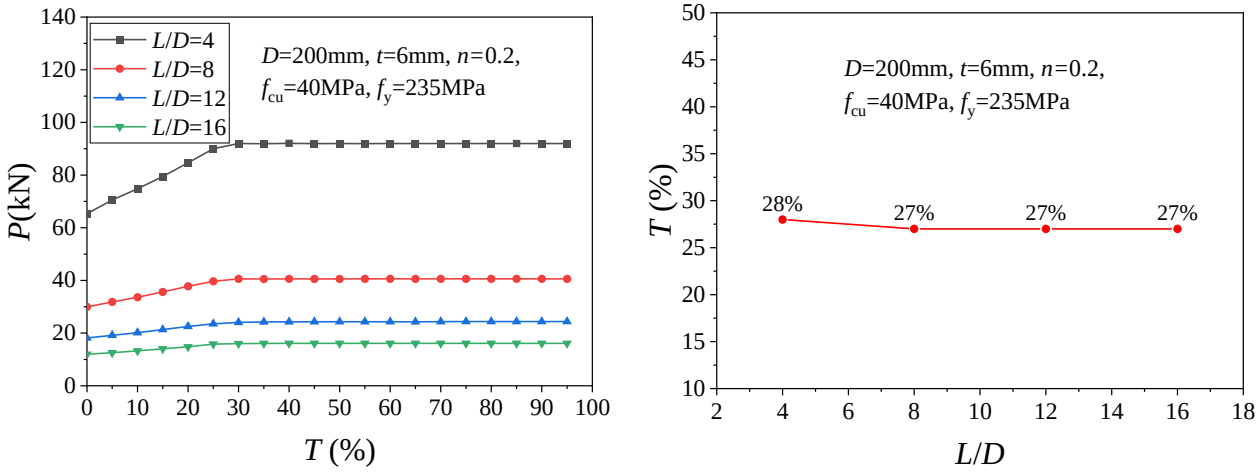

(a) Load capacity-concrete filling ratio curves (b) Optimal filling ratio under different aspect ratios

Fig. 17 Effect of aspect ratio on the load capacity and optimal filling ratio

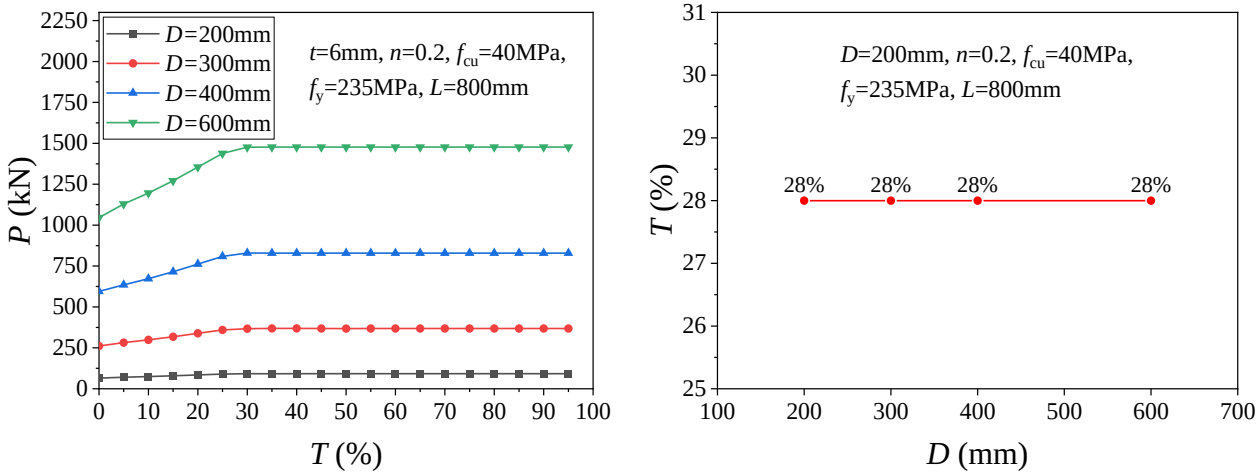

(a) Load capacity-concrete filling ratio curves (b) Optimal filling ratio under different section sizes

Fig. 18 Effect of section size on the load capacity and optimal filling ratio

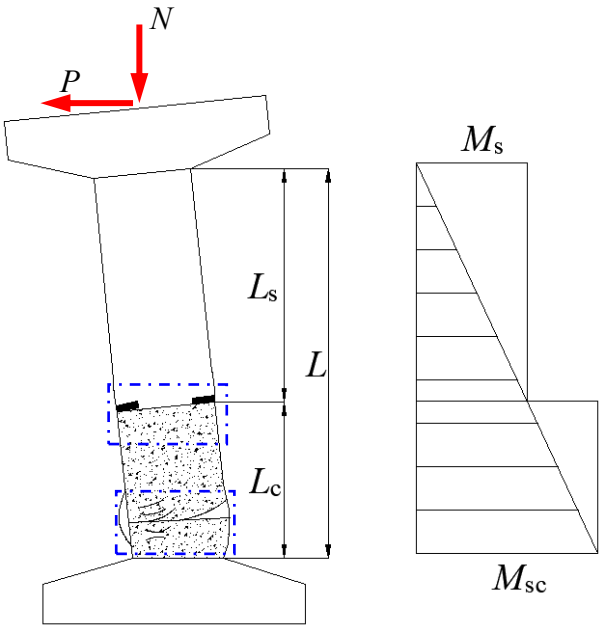

Fig. 19 Critical failure mechanism of partially CFST columns

(5) Aspect ratio

When the aspect ratio ranges from 4 to 16, the lateral load capacity is independent of the aspect ratios (Fig. 17(a)). Meanwhile, the aspect ratio has little effect on the optimal filling (Fig. 17(b)). This is because, within the considered parameter range, the change in aspect ratio has no effect on the strength of the two sections.

(6) Section size

Fig. 18(a) shows that when the section size ranges from 200mm to 600mm, the lateral load capacity increases with an increase in the section size. Fig. 18(b) illustrates the section size has no impact on the optimal filling ratio. This is because only changing the section dimension will lead to a proportional increase in the load capacity of both the SHS and the composite section.

3. Calculation method for the optimal filling ratio

3.1. Simplified mechanical model

When the aspect ratio of the column is greater than or equal to 4, the influence of cantilever shear deformation on structural performance can be ignored [32]. Therefore, compression-bending-shear components can be simplified as compression-bending components.

3.2. Calculation formulas for the optimal ratio

As mentioned before, the failure mode of partially CFST columns is characterized by a gradual transition from external buckling of the SHS to the formation of plastic hinges at the bottom of columns with increasing concrete filling ratio. At the critical point corresponding to the optimal filling ratio, as shown in Fig. 19, the SHS at the interface with the infilled concrete and the composite section at the bottom of column both reach their ultimate compression-bending capacity limits (i.e. M_1=M_s, and M_2=M_{sc}, where M_1 and M_2 correspond to the compression-bending capacity at the two respective sections in Fig. 19, M_s and M_{sc} represent the ultimate compression-bending capacity of the SHS and the composite section, respectively), which is also applicable to columns subjected to cyclic loading. Thus, the following equation can be obtained:

$$\frac{M_s}{L_s} = \frac{M_{sc}}{L} \tag{5}$$

where L_s is the length of the unfilled concrete within the steel tube, L_c is the

height of the infilled concrete, and L is the total length of the steel tube.

Based on the Eq. (5), the formula of optimal filling ratio can be further obtained in Eq. (6).

$$T_0 = 1 - \frac{M_s}{M_{sc}} \tag{6}$$

The compression-bending capacity of the composite section M_{sc} and the SHS M_s can be calculated according to Refs. [33] and [34], respectively.

3.3. Theoretical verification

3.3.1. Comparison between theoretical and FE results of section capacity

Comparisons between the theoretical values (M_s and M_{sc}) with the FE results (M_{sf} and M_{scf}) of the compression-bending capacity of the SHS and the CFST section are shown in Fig. 20. The average values of M_{sf}/M_s and M_{scf}/M_{sc} are 1.0583 and 1.0302, respectively, with variances of 0.0041 and 0.0050, respectively.

3.3.2. Comparison between theoretical and FE results of optimal filling ratio

The comparisons of optimal filling ratios between the theoretical calculation and FE analysis results under different parameters are shown in Fig. 21. It can be seen that they are in good agreement, indicating the theoretical formulas have a certain degree of good accuracy.

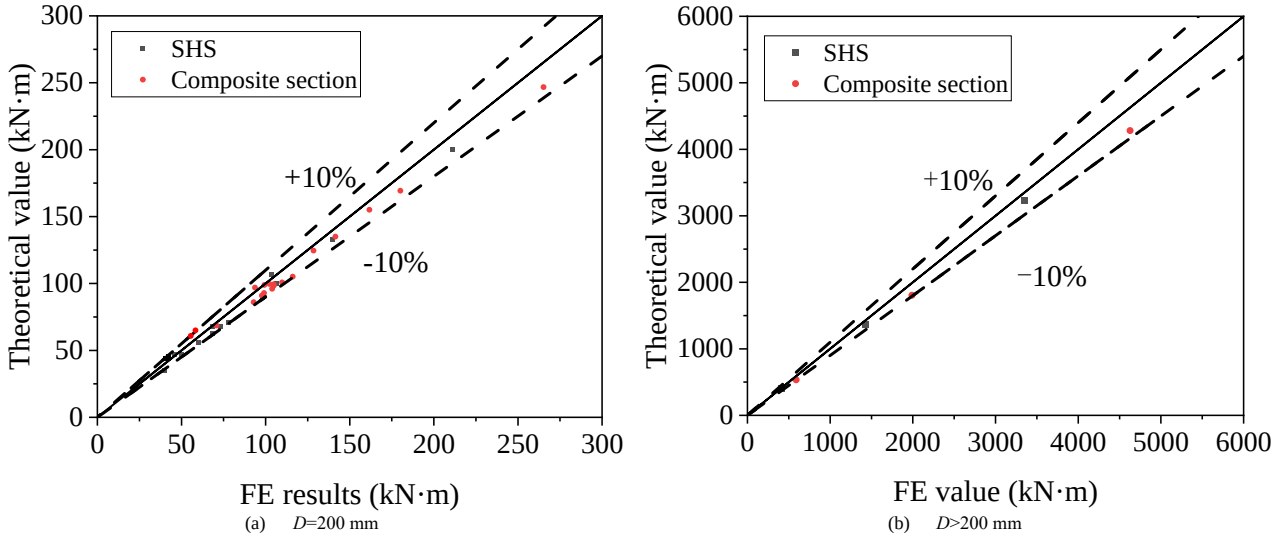

(a) D=200 mm (b) D>200 mm

Fig. 20 Comparison between theoretical and FE results

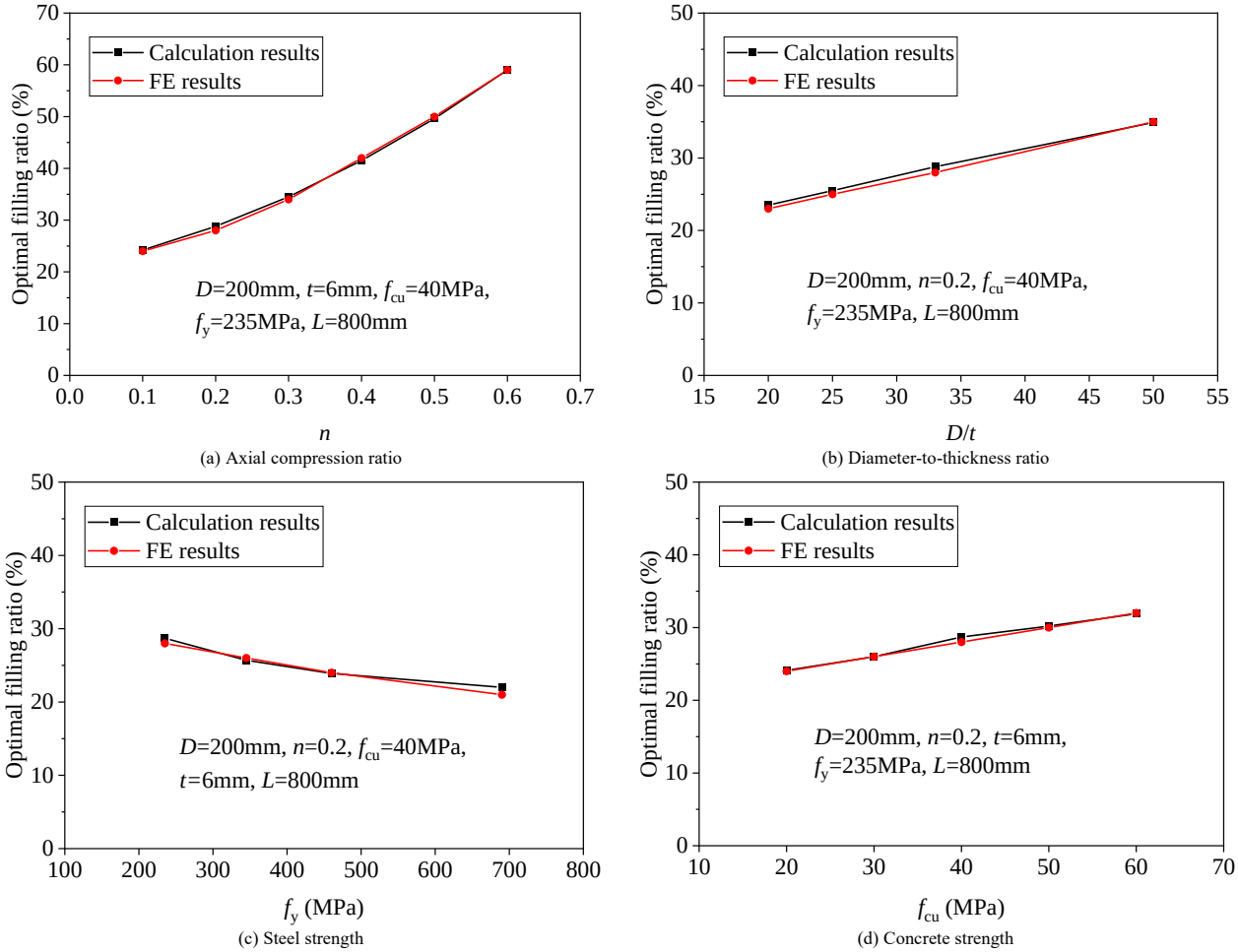

(a) Axial compression ratio (b) Diameter-to-thickness ratio

(c) Steel strength (d) Concrete strength

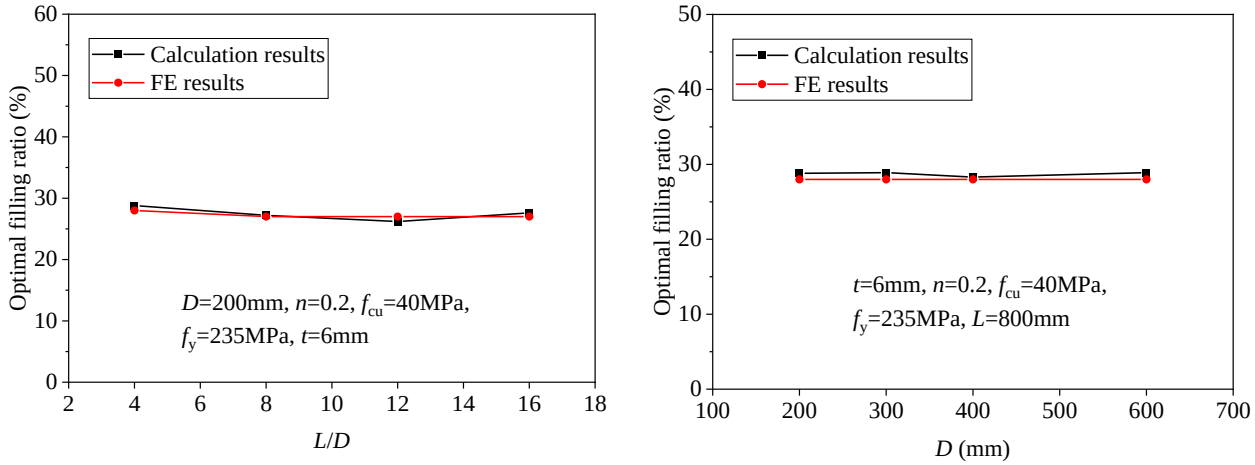

(e) Aspect ratio (f) Section size

Fig. 21 Optimal filling ratios of partially CFST columns between theoretical calculation and FE analysis result under different parameters

Table 3
Comparison between theory and experimental results in reference [34]

Specimen	*R* (mm)	*t* (mm)	*L* (mm)	Concretefilling ratio	Test results (kN)	Calcul-ation results(kN)	ratio	Optimal filling ratio (%)
SC34-66-00	140	4	1527	0	60.3	59.4	1.02	/
SC34-66-24	140	4	1527	24%	72.7	78.4	0.93	24.2%
SC34-66-28	140	4	1527	28%	71.7		0.92	
SC34-66-35	140	4	1527	35%	75.6		0.96	
SC26-85-00	180	4	1527	0	96.4	99.4	0.97	/
SC26-85-26	180	4	1527	26%	116.7	124.8	0.94	20.4%
SC26-85-35	180	4	1527	35%	116.1		0.93	
SC26-85-38	180	4	1527	38%	121.8		0.98	

3.3.3. Comparison between theoretical and experimental results of optimal filling ratio

The calculation results of the test specimens from Ref. [34] are presented in Table 3, and the failure mode is shown in Fig. 22. Using the calculation formula proposed in this paper, the optimal filling ratios of the partially CFST columns in Ref. [34] at two diameter-to-thickness ratios are listed in Table 3. This suggests that the failure mode after reaching the optimal filling ratio is the formation of plastic hinges at the bottom of column, which is consistent with the failure mode explained earlier.

4. Shear resistance of the transverse diaphragm

When a partially CFST column is subjected to combined axial compression and lateral loading, the interface shear needs to be transmitted from the steel tube to infilled concrete. Due to the reduced bond length of partially CFST columns, the natural bond strength between the steel tube and infilled concrete is significantly reduced, and necessary structural measures are required. Transverse diaphragms are critical structural elements to facilitate the composite effect between the steel tube and concrete in partially CFST columns. Therefore, it is necessary to analyze its transmission effect and load capacity.

4.1. FE model of columns with transverse diaphragms

4.1.1. Model description

The shear resistance of the transverse diaphragm was simulated through a push-out experimental model. In this model, an additional rigid loading plate was introduced, with a diameter 2mm smaller than the inner diameter of the steel tube and the point load was applied at the loading plate. All other settings are the same as Section 2. The FE model and boundary conditions are shown in Fig. 23.

4.1.2. Model verification

The shear resistance of the transverse diaphragm was simulated according to the Ref. [35], and the failure mode is shown in Fig. 24, where outward buckling occurred at the bottom of column. The comparison of load-displacement curves between the test results and the FE result is shown in Fig. 25. It can be seen that the FE model coincide effectively with the test.

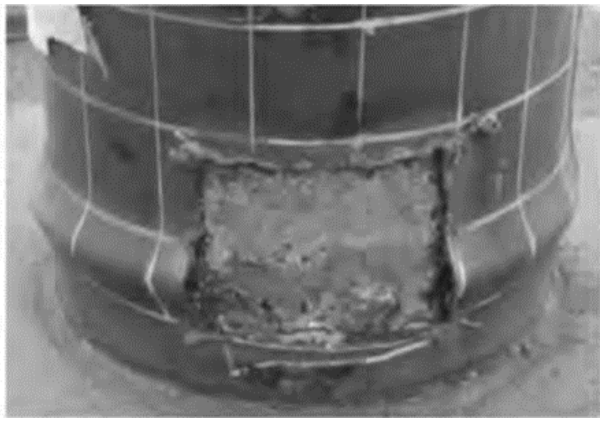

Fig. 22 Failure mode of SC-34-66-28

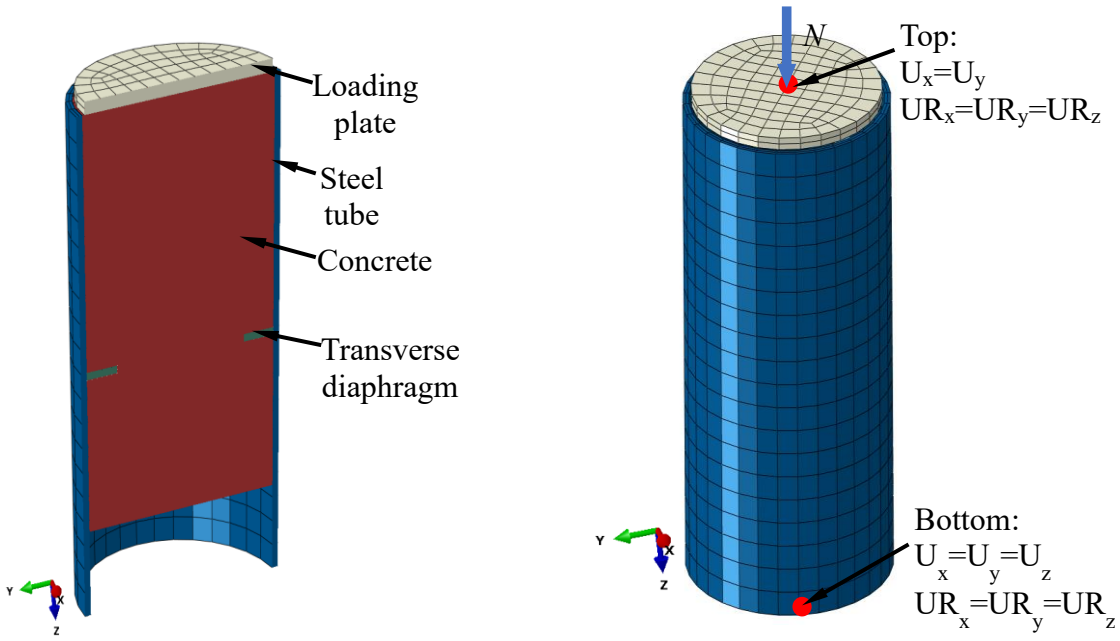

Fig. 23 FE model and boundary conditions

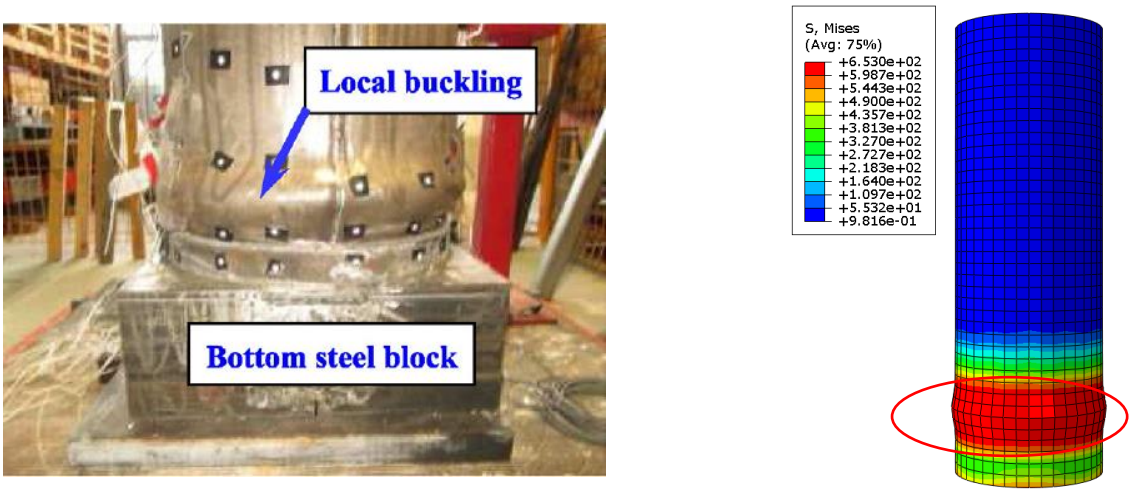

(a) Damage mode of CS400NR[35] (b)FE result

Fig. 24 Comparison of damage mode

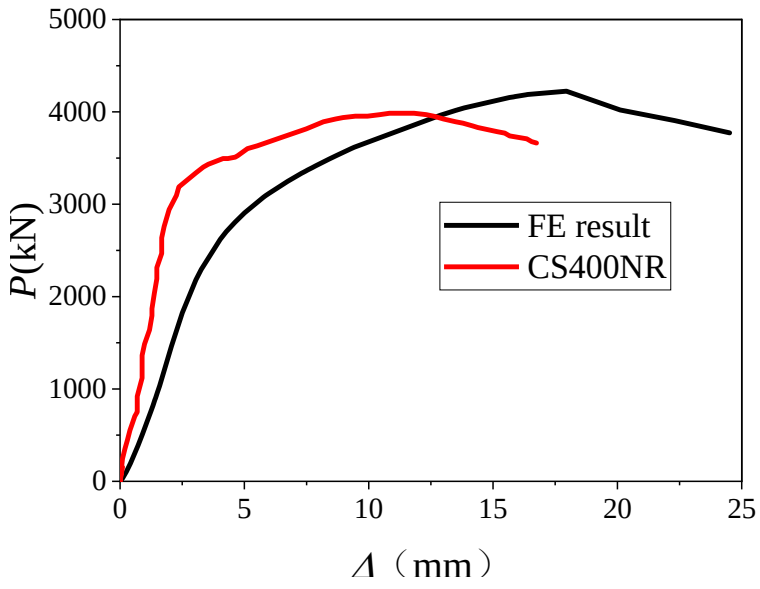

Fig. 25 Comparison of load-displacement curves

4.2. Parameter analysis

Akihiko Kono et al. [36] proposed a formula to calculate the shear strength P_d of a circular transverse diaphragm, as shown in Eq. (7). From the force analysis (Fig. 26), it can be seen that under axial load, the transverse diaphragm transfers the force from the concrete to the steel tube, and at this time, the

diaphragm is subjected to both pressure and reaction force.

$$P_{\mathrm{d}} = \varphi t_{\mathrm{d}} \frac{\sigma_y}{\sqrt{3}} \quad (7)$$

where φ is the inner circumference of the steel tube, t_{d} is the thickness of the circular transverse diaphragm, and σ_{y} is the yield strength of the circular transverse diaphragm.

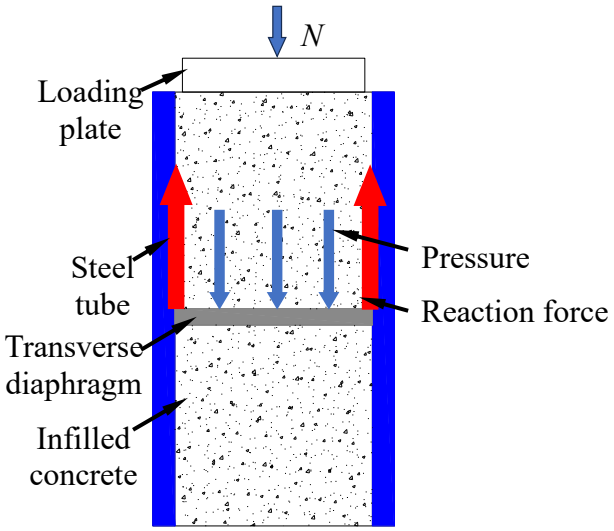

Fig. 26 Schematic diagram of the force acting on the transverse diaphragm

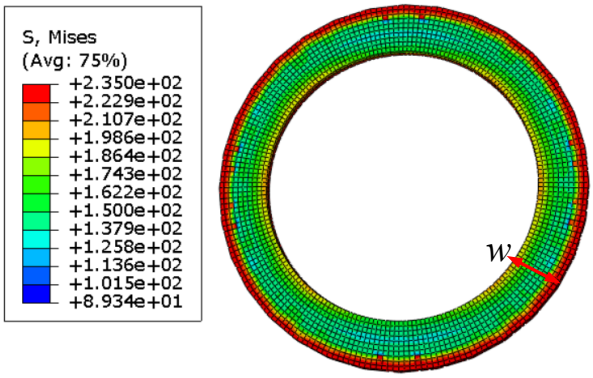

Fig. 27 The failure of transverse diaphragm

Table 4
Main parameters of the transverse diaphragms

Model Number	f_y (MPa)	t (mm)	d (mm)	w (mm)
q200-w30-t6-188	200	6	188	30
q235-w30-t6-188	235	6	188	30
q300-w30-t6-188	300	6	188	30
q355-w30-t6-188	355	6	188	30
q400-w30-t6-188	400	6	188	30
q460-w30-t6-188	460	6	188	30
q235-w30-t4-188	235	4	188	30
q235-w30-t5-188	235	5	188	30
q235-w30-t7-188	235	7	188	30
q235-w30-t8-188	235	8	188	30
q235-w30-t6-94	235	6	94	15
q235-w30-t6-282	235	6	282	45
q235-w15-t6-188	235	6	188	15
q235-w20-t6-188	235	6	188	20
q235-w25-t6-188	235	6	188	25
q235-w35-t6-188	235	6	188	35
q235-w40-t6-188	235	6	188	40
q235-w45-t6-188	235	6	188	45
q235-w50-t6-188	235	6	188	50

A preliminary simulation was conducted on the model, as shown in Fig. 27. It was inferred that the failure mode of the transverse diaphragm was shear failure at the edge. Therefore, when the transverse diaphragm fails, its shear load capacity is related to the strength of the weld seam or the strength of the welded part. Therefore, four parameters, namely, the strength, thickness, outer diameter and width of the transverse diaphragm, were selected for analysis.

Thus, 19 FE models were established as shown in the table 4, model designation conventions are explained using "q200-w30-t6-188" as an example: "q200" indicates a steel yield strength f_y =200 MPa, "w30" indicates that the width of the transverse diaphragm w=30 mm, "t6" denotes that the thickness of the steel tube t=6 mm, and "188" represents that the outer diameter of the transverse diaphragm d=188 mm. It should be noted that in order to achieve the failure of the transverse diaphragm, the cubic compressive strength f_{cu}=50MPa, the steel tube strength f_y=690MPa, and the diameter-to- thickness ratio (D/t) is set to 33.3, the length of the steel tube was taken as 400mm, the length of the concrete is 350mm, the transverse diaphragm was located in the middle of the steel tube. In order to obtain the load capacity of the transverse diaphragm, the contact between the concrete and steel tube interface and the concrete and transverse diaphragm interface was set to be frictionless.

4.2.1. Thickness

The load capacity of transverse diaphragm linearly increases with the thickness of transverse diaphragm as depicted in Fig. 28.

4.2.2. Strength

Fig. 29 depicts that the load capacity of transverse diaphragm linearly increases with yield strength (f_{y}).

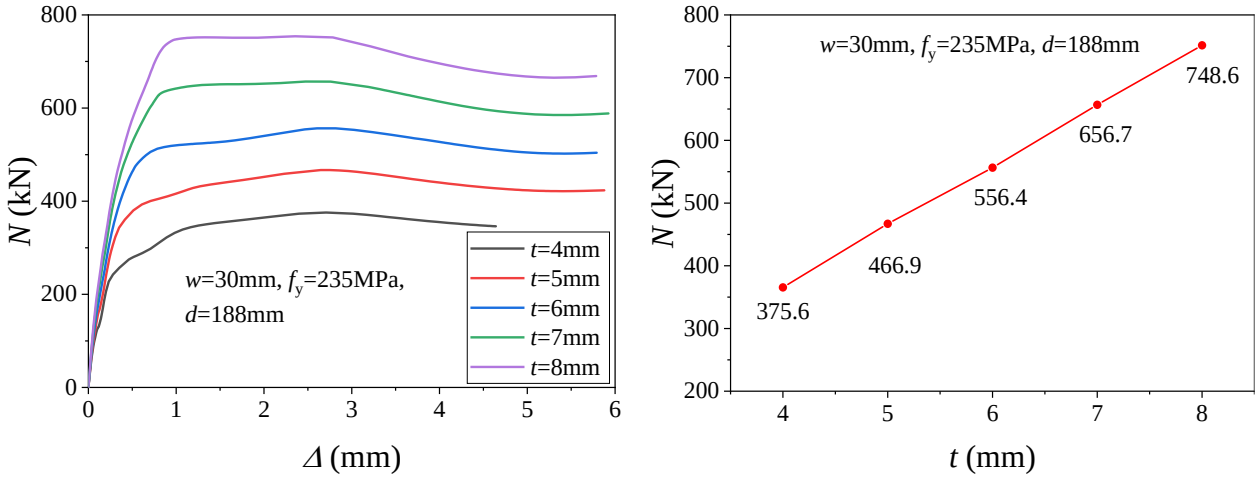

(a) Load-displacement curves of transverse diaphragms with different thicknesses (b) Load capacity of transverse diaphragms with different thicknesses

Fig. 28 The effect of thickness on the load capacity of transverse diaphragms

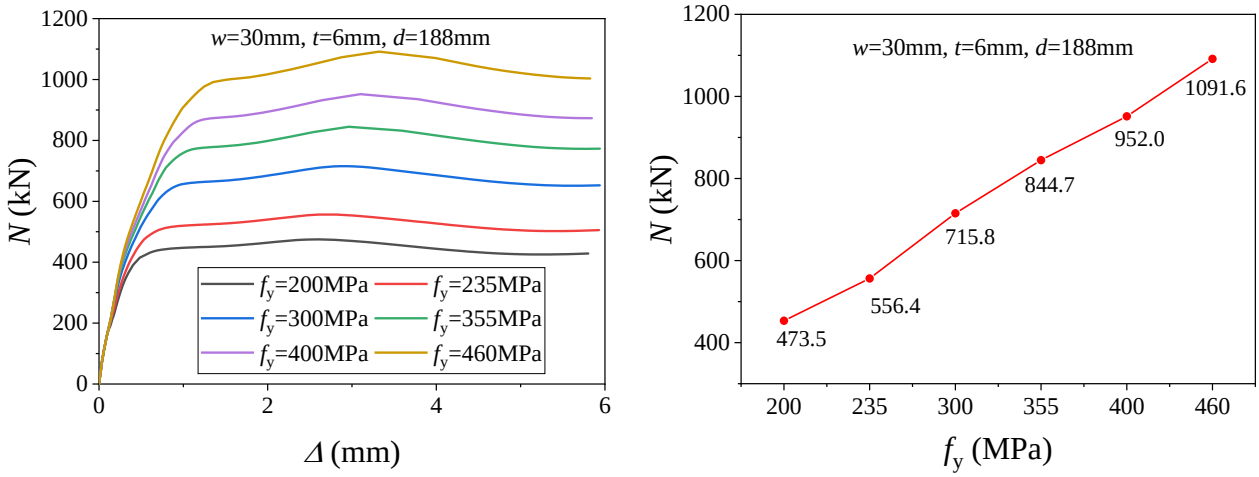

(a)Load-displacement curves of diaphragm under different strengths (b) Load capacity of transverse diaphragms with different strengths

Fig. 29 Effect of strength on the load capacity of transverse diaphragms

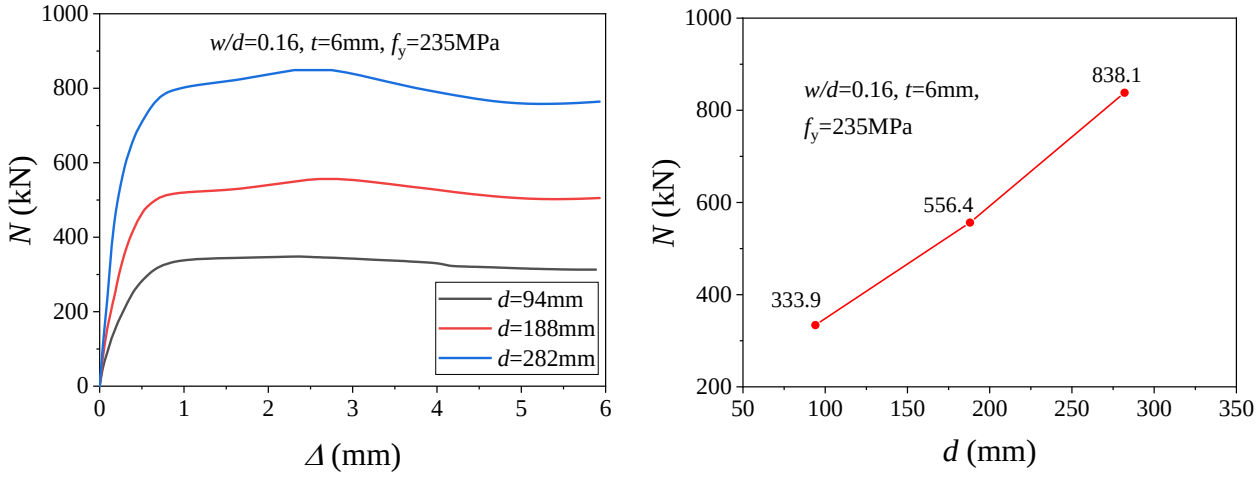

(a) Load-displacement curves of diaphragm under different outer diameters (b) Load capacity of transverse diaphragms with different outer diameters

Fig. 30 Effect of outer diameter on the load capacity of transverse diaphragms

4.2.3. Outer diameter of the diaphragm

Fig. 30 depicts when the outer diameter of the transverse diaphragm ranges from 94mm to 282mm, the transverse diaphragm load capacity almost linearly increases with transverse diaphragm strength.

4.2.4. Width

The load capacity suddenly increases when the width of the transverse diaphragm increases from 15mm to 20mm (The corresponding ratio of diaphragm area to concrete area ranges from 0.38 to 0.29), while further increasing the width does not significantly improve the load capacity (Fig. 31). The reason is that the compressed concrete area is too small, its load capacity is insufficient, and the concrete is crushed. Therefore, in order to prevent concrete from being crushed, the width of the diaphragm must be controlled. Ref. [37] reported that the annular compression area in steel tube concrete shall not be less than 1/3 of the concrete section, which is consistent with the FE results. In summary, the width of the transverse diaphragm is not considered as the main influencing factor, but it should not be too small, it is recommended to set the area of the transverse diaphragm to 1/3 of the concrete cross-sectional area, conservatively taking, w=0.1d.

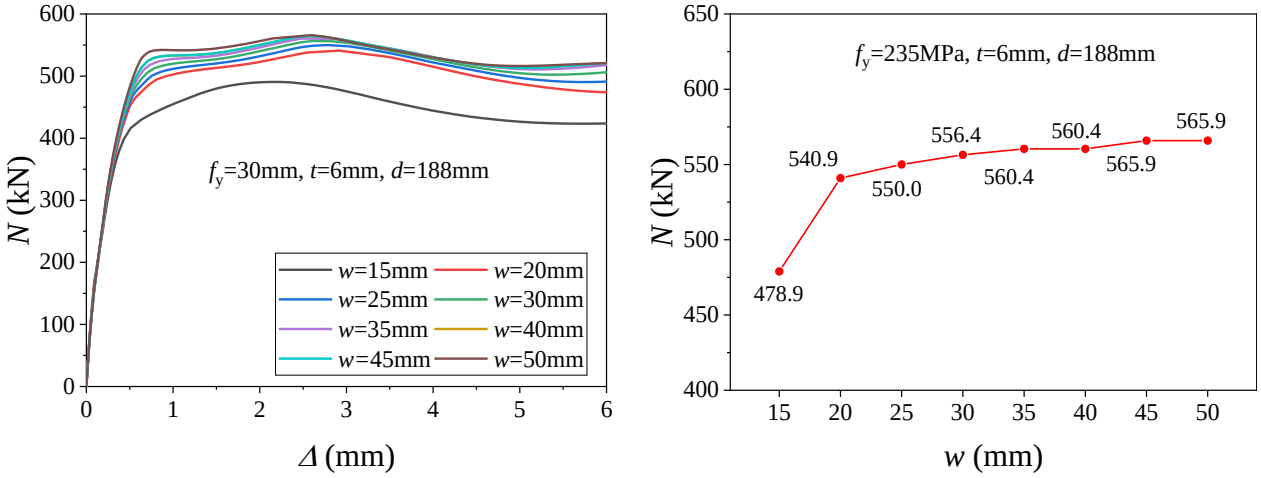

(a) Load-displacement curves of transverse diaphragms with different widths (b) Load capacity of transverse diaphragms with different widths

Fig. 31 Effect of width on the load capacity of transverse diaphragms

4.3. Design method for transverse diaphragms

4.3.1. Transverse diaphragm load capacity

The load capacity of the transverse diaphragm is primarily proportional to thickness, strength, and perimeter length of the transverse diaphragm. The FE results were compared with the formula calculation results, as shown in Fig. 32. It can be seen that Eq. (7) is relatively conservative and can be used to predict the load capacity of the diaphragm.

4.3.2. Load capacity reduction factor ω

When the partially CFST column is subjected to the combined lateral and axial loads, the equivalent plastic strain nephogram of concrete under peak load is shown in Fig. 33, and it can be seen that the failure of concrete is mainly concentrated in the compression zone, indicating that the concrete here loads a large force, while the concrete in the tension zone is almost not subjected to force. Additionally, as shown in Fig. 34, the transverse diaphragm reaches yield in the compression zone, but the stress in the tension zone is basically small. Therefore, the force acting on the transverse diaphragm decreases uniformly along the negative y-axis direction, as shown in Fig. 35, and the reduction factor is defined as ω. ω can be calculated as Eq. (8), and the calculated reduction factor of transverse diaphragm is 0.5.

$$\omega = \left(\frac{2\int_0^{\frac{\pi}{2}} R\cos\theta d\theta}{R} + \frac{2\int_{-\frac{\pi}{2}}^{0} 1-R\cos\theta d\theta}{-R}\right)/2\pi \quad (8)$$

Therefore, the load capacity of the transverse diaphragm in partially CFST column under combined lateral and axial loads can be obtained from Eq. (9).

$$P_{c1} = 0.5\varphi t_d \frac{\sigma_y}{\sqrt{3}} \quad (9)$$

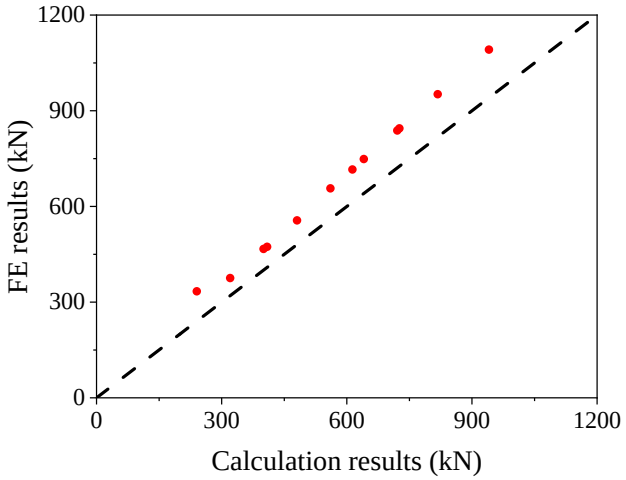

Fig. 32 Comparison between theory results and FE results

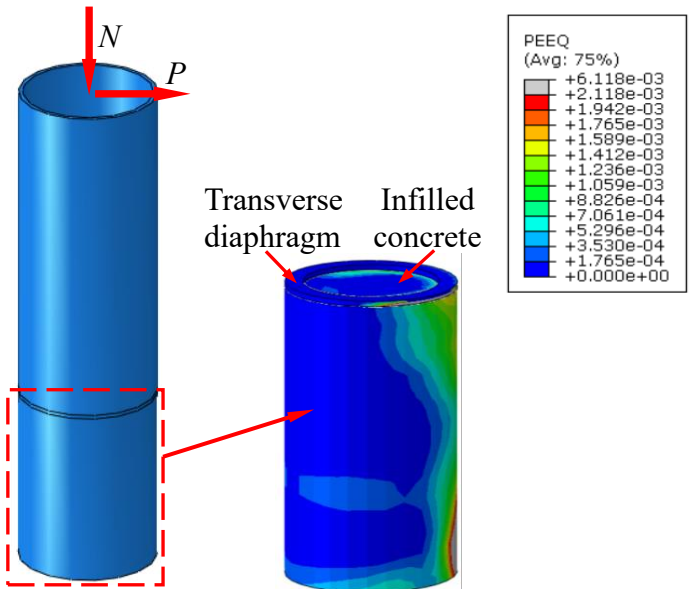

Fig. 33 Equivalent plastic strain nephogram of concrete under peak load

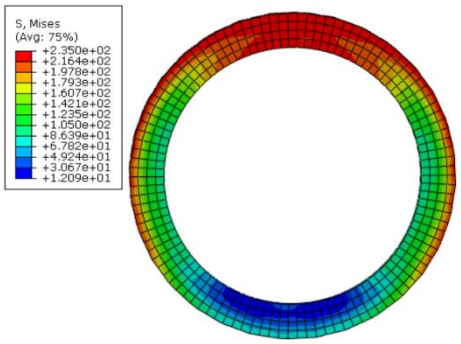

Fig. 34 Stress nephogram of the transverse diaphragm

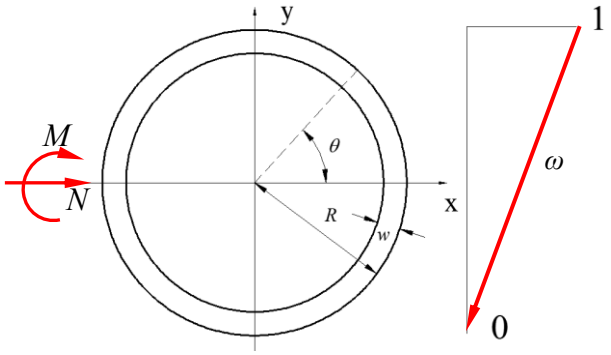

Fig. 35 Schematic diagram of reduction factor ω

5. Interface shear demand and design procedure

5.1. Shear demand in partially CFST columns

From the force analysis shown in Fig. 36, it is evident that under combined lateral and axial loads, the interface shear force exists between the inner wall of the steel tube and the surface of the infilled concrete. The interface shear resistance should be greater than the shear demand, so the transverse diaphragms are sufficient to transfer the load to the infilled concrete, allowing the infilled concrete to be fully utilized. Note that the contribution of friction is ignored and used as a strength reserve.

The calculation of the plastic load capacity of the composite section is based on the following assumptions:

(1) At the ultimate limit state, transverse diaphragms can effectively transfer the shear force between the steel tube and infilled concrete.

(2) The tensile resistance of the concrete is neglected.

(3) The plane remains plane.

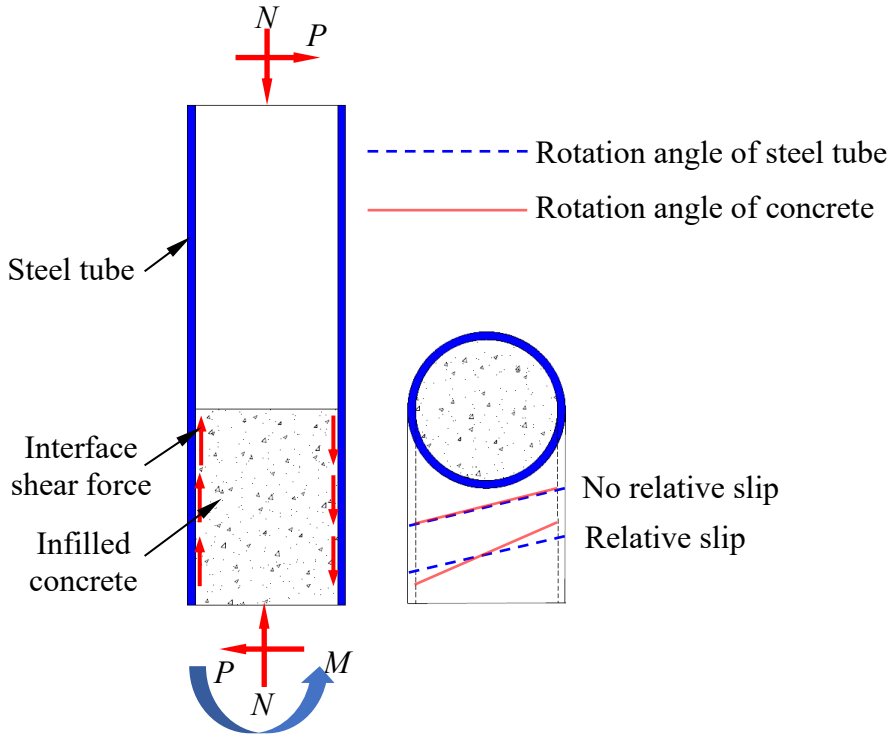

Fig. 36 Schematic diagram of mechanism analysis under lateral and compression loads

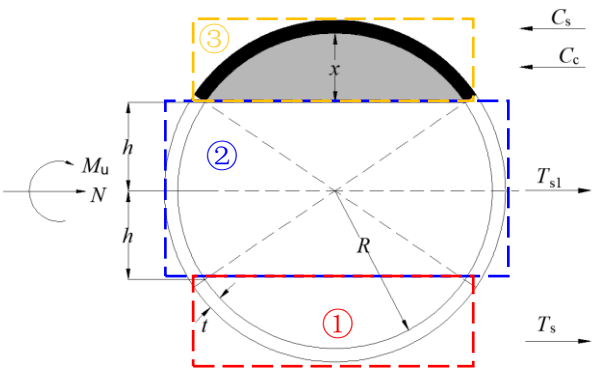

Fig. 37 Force conditions of circular composite section under compression-bending state

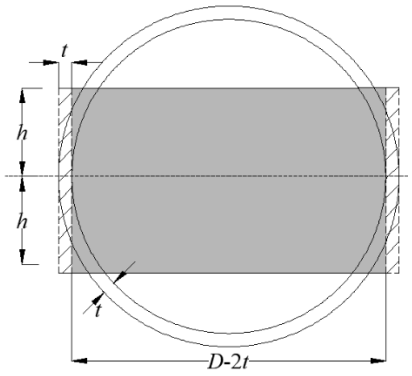

Fig. 38 Simplified calculation diagram

5.2. Calculation of shear demand for circular composite sections

Fig. 37 shows the force diagram of a circular composite section under compression and bending, for ease of explanation, the section is divided into three zones: ①, ②, ③. And the equilibrium equation of the force ($\sum F$=0) is obtained:

$$C_s + C_c - T_s - T_{s1} - N = 0 \tag{10}$$

where C_c is the axial compressive resistance of the compressed concrete, C_s is the axial compressive resistance of the steel tube in zone ③, T_s is the tensile force of the steel tube in zone ①, T_{s1} is the tensile force of the steel tube in zone ②.

As shown in Fig. 37, zone ① and zone ③ are completely symmetrical, therefore, Eq. (11) can be obtained:

$$C_s = T_s \tag{11}$$

Simultaneous Eq. (10) and (11)

$$N = C_c - T_{s1} \tag{12}$$

As shown in Fig. 38, simplify the concrete area within the 2h range to the gray area and simplify the steel tube area within the 2h range to the shaded area (h is the distance from neutral axis to central axis). Therefore, C_c and T_{s1} can be expressed as

$$C_c = (\frac{\pi D^2}{8} - hD) f_c' \tag{13}$$

$$T_{s1} = 4thf_y \tag{14}$$

where, f_c' is the cylinder compressive strength of concrete, t is the thickness of the steel tube, D is the inner diameter of the steel tube, R is the inner radius of the steel tube.

Eq. (12), Eq. (13) and Eq. (14) are combined to calculate h, as shown in Eq. (15).

$$h = \frac{\frac{\pi D^2}{8} f_c' - N}{f_c' D + 4tf_y} \tag{15}$$

The above calculations are based on the compression zone being above the centerline of the section. At this point, the height of the compression concrete zone is

$$x = R - h \tag{16}$$

Then, substitute Eq. (15) into Eq. (16):

$$x = R + \frac{N - \frac{\pi D^2}{8} f_c'}{f_c' D + 4tf_y} \tag{17}$$

when the height of the compression zone x is greater than the radius R, the result remains unchanged.

The shear demand for composite sections is

$$N_v = A_c' f_c' \tag{18}$$

where A_c' is the concrete area in compression zone, and A_c' can be determined by Eqs. (19) and (20).

$$A_c' = (\beta R^2 - R\sin\beta)/2 \tag{19}$$

$$\beta = \arcsin\frac{h}{R} \tag{20}$$

5.3. Calculation verification

Fig. 39 shows a schematic diagram of the composite section under combined axial and lateral loads. The calculation of the compression-bending capacity for circular composite section corresponding to the shear demand is as follows:

$$M_c = A_c' f_c' y_{st} + 4f_y \int_{\alpha}^{\frac{\pi}{2}} R_0^2 t \sin\theta d\theta = \frac{2}{3}\left(\frac{h}{\tan\alpha}\right)^3 f_c' + 4\cos\alpha R_0^2 t f_y \tag{21}$$

where y_{st} is the distance from the central axis for C_c, R_0 is the radius of the center surface of the steel tube, α is the angle in radians between the edge of the compression zone and the positive direction of the x-axis.

The comparison between the calculated results (M_c) based on shear demand and the theoretical values (M_{ch}) are shown in Table 5. The average ratio of M_c/M_{ch} is 0.9453, with a variance of 0.00089. The results indicate that the calculated results agree well with the theoretical values.

Table 5
Comparison of calculated values with theoretical values

Model Number	Composite section		
	M_c (kN·m)	M_{ch} (kN·m)	M_c/M_{ch}
C235-n1-200-4-33-32	64.92	70.19	0.9249
C235-n2-200-4-33-32	67.98	71.59	0.9496
C235-n3-200-4-33-32-	70.35	73.58	0.9561
C235-n4-200-4-33-32	71.89	73.13	0.9830
C235-n5-200-4-33-32	72.52	72.09	1.0060
C235-n6-200-4-33-32	72.21	70.38	1.0260
C235-n2-400-4-33-32	538.70	588.77	0.9150
C235-n2-600-4-33-32	1811.47	1989.22	0.9106
C235-n2-800-4-33-32	4285.51	4626.42	0.9263
C235-n2-200-4-20-32	102.05	109.17	0.9348
C235-n2-200-4-25-32	85.64	91.37	0.9373
C235-n2-200-4-50-32	49.15	53.44	0.9197
C355-n2-200-4-33-32	97.76	101.51	0.9631
C460-n2-200-4-33-32	122.77	130.57	0.9403
C690-n2-200-4-33-32	175.14	185.36	0.9449
C235-n2-200-4-33-20	62.55	67.79	0.9227
C235-n2-200-4-33-30	65.68	70.70	0.9290
C235-n2-200-4-33-50	69.90	74.91	0.9331
C235-n2-200-4-33-60	72.01	76.80	0.9376
	Average value		0.9453
	Variance		0.00089

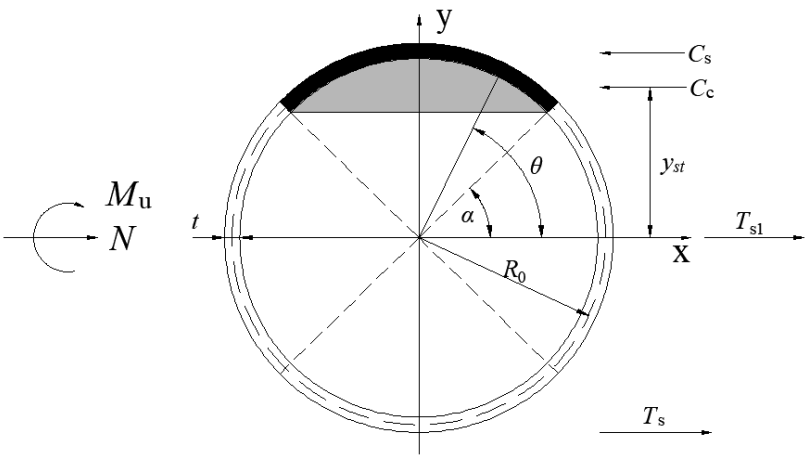

Fig. 39 Schematic diagram for calculating compression-bending capacity of circular composite section

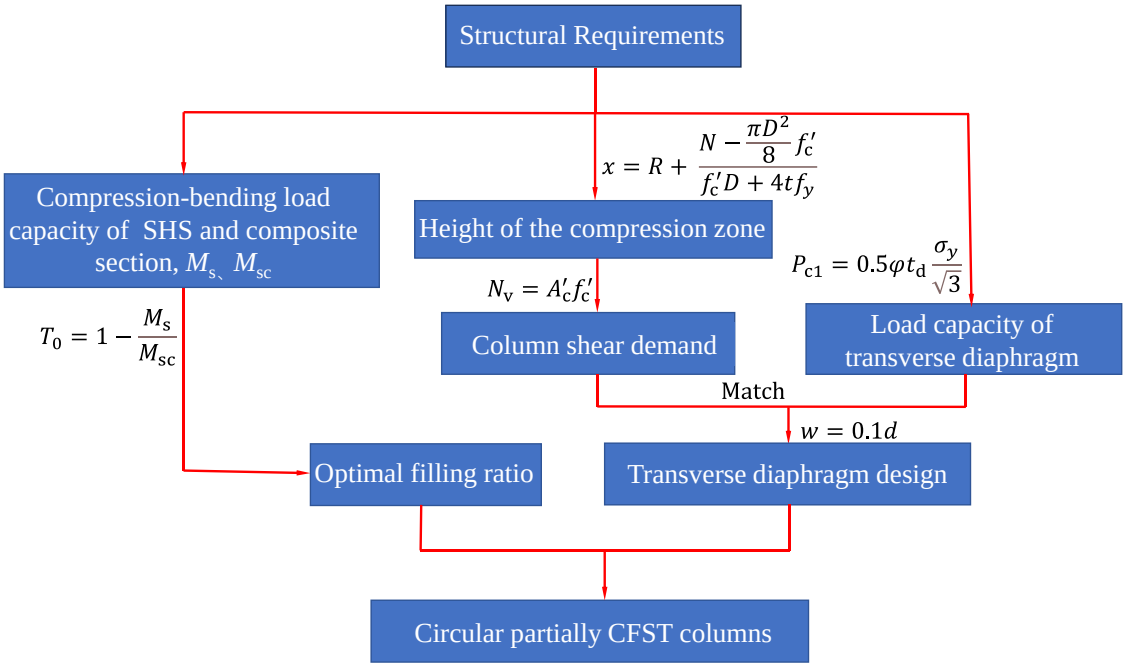

Fig. 40 Design procedure for partially CFST columns

5.4. Design procedure

Base on the comprehensive analysis of the mechanism of partially CFST columns, the main process is shown in Fig. 40. Firstly, based on the known engineering conditions and structural requirements, specific parameters for the partially CFST columns can be designed. Secondly, the optimal filling ratio can be calculated from the compression-bending capacity of the SHS and composite section using Eq. (6). Then, the shear demand of the partially CFST columns can be computed from the column dimensions, materials, and load conditions using Eq. (17) and Eq. (18). Finally, With Eq. (9), design recommendations for w=0.1d, considering the dimensions, and shear demand of the partially CFST columns, the design parameters for the transverse diaphragms can be determined. The design process concludes with the establishment of the concrete filling ratio and transverse diaphragm design, completing the design procedure for the partially CFST columns.

6. Conclusions

This study comprehensively discusses the influence of various parameters on the load capacity and optimal filling ratio of partially CFST columns. Based on the extensive FE and theoretical analysis of partially CFST column, the following observations and conclusions can be drawn:

(1) The concrete filling ratio can alter the failure mode of circular partially CFST columns subjected to combined constant axial compression and lateral loading. With an increase in the concrete filling ratio, the failure position shifts from the SHS above the filling interface to the bottom composite section.

(2) Prior to reaching the optimal concrete filling ratio, the load capacity, ductility, and stiffness of partially CFST columns increase with increasing concrete filling ratio. After reaching the optimal filling ratio, the load capacity and ductility remain relatively constant, but the stiffness increases.

(3) The optimal filling ratio of partially CFST columns under combined compression and lateral loads increases with increasing axial compression ratio, diameter-to-thickness ratio and concrete strength but decreases with increasing steel material strength. However, it is largely unaffected by the aspect ratio and section size.

(4) Transverse diaphragms transfer interface shear force, and the load capacity of transverse diaphragms is linearly related to the thickness, strength, and outer diameter of the transverse diaphragms. The calculation formulas for the load capacity of the transverse diaphragm in partially CFST columns was proposed. Additionally, it is recommended to use 0.1 times the outer diameter of the transverse diaphragm as the width of the transverse diaphragm.

(5) The interface shear demand in partially CFST columns was theoretically derived. By matching the shear demand with the load capacity of the transverse diaphragm, the design of the transverse diaphragm can be determined.

(6) The design procedure that can facilitate their wider applications for partially CFST columns was summarized and proposed, in which the optimal filling ratio and transverse diaphragm dimensions are main parameters.

Future research should focus on the application and optimized design of partially CFST columns in frame structures.

Acknowledgments

The authors greatly appreciate the financial support provided by the National Natural Science Foundation of China (No. 52378133) and Chongqing Natural Science Foundation of China (No. CSTB2023NSCQ-MSX0758). However, the opinions expressed in this work are solely the authors' own.

References

[1] Report on the Hanshin-Awaji earthquake disaster-damage to civil engineering. Tokyo: Maruzen Co, Ltd, 1996 [in Japanese].
[2] Li GC, Chen BW, Zhu BW, Yang ZJ, Ge HB, Liu YP. Axially loaded square concrete-filled steel tubular long columns made of high-strength materials: Experimental investigation, analytical behavior and design. J Build Eng 2022;58:104994.
[3] Du ZL, Liu YP, He JW, Chan SL. Direct analysis method for noncompact and slender concrete-filled steel tube members.Thin Wall Struct 2019;135:173-184.
[4] Li GC, Yang Y, Yang ZJ, Fang C, Ge HB, Liu YP. Mechanical behavior of high-strength concrete filled high-strength steel tubular stub columns stiffened with encased I-shaped CFRP profile under axial compression. Compos Struct 2021;275: 114504.
[5] Chan SL, Liu YP, Liu SW, A New Codified Design Theory of Second-order Direct Analysis for Steel and Composite Structures – From Research to Practice. Structures 2017; 9: 105-111.
[6] Li GQ, Chen BW, Yang ZJ, Ge HB and Li X. Axial behavior of high-strength concrete-filled high-strength square steel tubular stub columns. Adv Steel Constr 2021;17(2):158-168.
[7] Li GC, Qiu ZM, Yang ZJ, Chen BW and Feng YH. Seismic performance of high strength concrete filled high strength square steel tubes under cyclic pure bending. Adv Steel Constr 2020;16(2):112-123.
[8] Zhou XH, Gan D, Liu JP and Chen YF. Composite effect of stub square steel tubed columns under axial compression. Adv Steel Constr 2018;14(2):274-290.
[9] Li GC, Liu XH, Yang ZJ, Fang C, Ge HB, Liu YP. Testing, modeling, and design of square CFST columns internally reinforced by pultruded CFRP profile under axial compression. Eng Struct 2022;273: 115110.
[10] Li GC, Sun X, Yang ZJ, Fang C, Chen BW, Ge HB, Liu YP. Structural performance of concrete-filled square steel tubular columns encased with I-shaped CFRP under eccentric compression. Eng Struct 2021;248: 113254.
[11] Kang WH, Uy B, Tao Z and Hicks S. Design strength of concrete-filled steel columns. Adv Steel Constr 2015;11(2):165-184.
[12] Kitadt T. Ultimate strength and ductility of state-of-the-art concrete-filled steel bridge piers in Japan. Eng Struct 1998; 20(4-6): 347-354.
[13] Gan D, Zhang YJ, Zhou XH, Zhang XJ. Investigation of cyclic behavior of partially concrete-filled steel tubular columns, Eng Struct 2024; 300: 117175.
[14] Goto Y, Ebisawa T, Lu XL. Local Buckling Restraining Behavior of Thin-Walled Circular CFT Columns under Seismic Loads. J Struct Eng 2012; 140(5): 04013105.
[15] Yuan H, Dang J, Aoki T. Experimental study of the seismic behavior of partially concrete-filled steel bridge piers under bidirectional dynamic loading. Earthq Eng Struct D 2013; 42: 2197-2216.
[16] Yuan H, Dang J, Aoki T. Behavior of partially concrete-filled steel tube bridge piers under bidirectional seismic excitations. J Constr Steel Res 2014; 93(2): 44-54.
[17] Goto Y, Ghosh P, Kawanishi N. Nonlinear Finite Element Analysis for Hysteretic Behavior of Thin-Walled Circular Steel Columns with In-Filled Concrete. J Struct Eng, 2010; 136(11): 1413-1422.
[18] Goto Y, Mizuno K, Ghosh P. Nonlinear finite element analysis for cyclic behavior of thin-walled stiffened rectangular steel columns with in-filled concrete. J Struct Eng 2012; 138(5): 571-584.
[19] Lai ZC, Varma AH. Seismic behavior and modeling of concrete partially filled spirally welded

pipes. Thin Wall Struct 2017; 113: 240-252.
[20] Xiang NL, Yang F, Xu C. Novel fiber-based seismic response modeling and design method of partially CFST bridge piers considering local buckling effect. Soil Dyn Earthq Eng 2023; 170: 107911.
[21] Khalifa M, Shaat A, Ibrahim S. Optimum concrete filling ratio for partially filled noncompact steel tubes. Thin Wall Struct 2019; 134: 159-173.
[22] Wang ZF, Sui WN, Zhao ZH Pang H, Liao J. Study on seismic performance of partially concrete-filled steel circular bridge piers with transverse diaphragm. J Build Struct 2013; 34(S1): 233-239(in Chinese).
[23] Usami T, Ge HB, Saizuka K. Behavior of partially concrete-filled steel bridge piers under cyclic and dynamic loading. J Constr Steel Res 1997; 41(2-3): 121-136.
[24] Usami T, Ge HB. Ductility of concrete-filled steel box columns under cyclic loading. J Struct Eng 1994; 120(7): 2021-2040.
[25] Ge HB, Usami T. Cyclic tests of concrete-filled steel box columns. J Struct Eng 1996; 122(122): 1169-1177.
[26] Kwon YB, Song JY, Kon KS. The structural behavior of concrete filled steel piers. Proceedings of 16th Congress of IABSE. Iucerne, Switzerland: University of Applied Sciences Fribourg,2000; 16(18): 115-154.
[27] Zhou XH, Cheng GZ, Liu JP, Gan D, Chen YF. Behavior of circular tubed-RC column to RC beam connections under axial compression. J Constr Steel Res 2017; 130: 96-108.
[28] Li GC, Chen BW, Yang ZJ, Liu YP, Feng YH. Experimental and numerical behavior of eccentrically loaded square concrete-filled steel tubular long columns made of high-strength steel and concrete. Thin Wall Struct 2021;159: 107289.
[29] Zhou XH, Zhou Z, Gan D. Analysis and design of axially loaded square CFST columns with diagonal ribs. J Constr Steel Res 2020; 167: 105-848.
[30] Han LH, Yao GH, Tao Z. Performance of concrete-filled thin-walled steel tubes under pure torsion. Thin Wall Struct 2007; 45(1):24-36.
[31] Han LH. Concrete filled steel tubular structures: Theory and Practice. 3rd ed. Beijing：Science Press, 2016: 253-261 [in Chinese].
[32] 'International Federation for Structure Concrete. Model Code for Concrete Structures 2010: CEB-FIP MC90. Lausanne: International Federation for Structure Concrete, 2013.
[33] Tong GS. In-plane Stability of Steel Structures [M]. Beijing: China Construction Industry Press, 2015 [in Chinese].
[34] Wang ZF, Sui WN, Li GC, Wu Q, Ge L. Mechanical behavior of partially concrete-filled steel circular bridge piers under cyclic lateral load. China J High Transp 2015; 28(1): 62 - 70 [in Chinese].
[35] Tao Z, Song TY, Uy B, Han LH. Bond behavior in concrete-filled steel tubes. J Constr Steel Res 2016; 120:81-93.
[36] Akihiko K, Kenji S, Yuki O, et al. A quantitative evaluation of the stress transfer effect between steel tube and infill concrete by horizontal diaphragms in a CFST column. Architec Inst Jpn 2005; 598: 163-167 [in Japanese].
[37] Xue LH, Cai SH. Experimental study on bearing strength of concrete near the interface of steel tube and concrete core. Build Sci 1998; 04: 9-13+18 [in Chinese].